Arch Virol (2008) 153:1605–1609
DOI 10.1007/s00705-008-0156-0

BRIEF REPORT

Lack of vertical transmission of Hantaan virus from persistently infected dam to progeny in laboratory mice

Midori Taruishi · Kumiko Yoshimatsu · Rei Hatsuse · Megumi Okumura · Ichiro Nakamura · Jiro Arikawa

Received: 22 June 2007 / Accepted: 9 June 2008 / Published online: 9 July 2008

Abstract It is unclear how the hantaviruses are transferred from infected to uninfected rodents. We studied the status of persistently infected laboratory mice and examined the frequency of viral transmission to their offspring. Expression of Hantaan virus nucleocapsid protein was detected in the lungs of persistently infected dams. None of the progeny displayed viral antigen, although they were strongly positive for IgG antibodies against hantavirus. There was neither hantavirus RNA nor virus-specific IgM antibodies or virus-specific $CD8^+$ T cells in the progeny. These results did not show any indication for a vertical transmission of hantaviruses, at least in the laboratory mouse model studied.

Hantaviruses comprise the genus *Hantavirus* in the family *Bunyaviridae*. Although hantaviruses cause two serious and often fatal human diseases, viz. hemorrhagic fever with renal syndrome (HFRS) and hantavirus pulmonary syndrome (HPS), their natural rodent hosts present no obvious clinical signs of infection. Instead, they carry the virus for long periods as reservoir animals and shed the virus into excreta such as urine, feces, and saliva [16]. An age-dependent increase in the infection rate was recently identified by epizootiological surveillance in a rodent colony [4, 6], suggesting that these viruses are maintained by horizontal transmission through close contact between adult rodents and not by vertical transmission to neonates from dams.

Several studies have demonstrated the protective effect of hantavirus-specific antibodies in rat fetuses from or neonates born to immune mothers. Neonates that received a lethal dose of Seoul virus (SEOV) strains B-1 or SR-11 intraperitoneally within 24 h or at 2 days after birth to immune dams survived [10, 23]. These results imply that the neonates were protected against infection by transfer of maternal anti-hantavirus antibodies. However, these reports did not address whether the mother rats were persistently infected during pregnancy and the nursing period. In addition, given the difficulty of analyzing young animals in nature, the existence of vertical transmission from persistently infected animals to their offspring remains unclear.

There are several animal models of persistent infection involving hantaviruses and their natural reservoir species of rodents, including SEOV-infected rats [7, 19], Hantaan virus (HTNV)-infected *Apodemus* mice [15], Black Creek Canal virus-infected cotton rats [12], and Sin Nombre virus-infected deer mice [5]. These model rodents harbor virus antigen for a long time without signs of disease, as wild rodents do. However, since there is little genetic information on natural rodent species, it has often been difficult to analyze the mechanism of persistent infection genetically. Previously, we established a persistent infection model in laboratory mice. Viral antigen was detected in the lungs of the animals until 90 days after infection without signs of disease [2], and the retention time of the viral antigen was dependent on their age at inoculation [3]. A weak antigen-specific cytotoxic T lymphocyte (CTL) response was detected in these laboratory mice following infection [2, 20]. Although laboratory mice are not the natural reservoir, the persistently infected mice mimic the natural reservoir hosts in important aspects: (1) they have

M. Taruishi · K. Yoshimatsu · R. Hatsuse · M. Okumura · I. Nakamura · J. Arikawa (✉)
Institute for Animal Experimentation, Hokkaido University Graduate School of Medicine, Kita-ku, Kita-15, Nishi-7, Sapporo 060-8638, Japan
e-mail: j_arika@med.hokudai.ac.jp

large amounts of virus antigen in their lungs [2], (2) they do not show obvious signs of disease in the persistent infection phase [20], and (3) the virus is not eliminated, although persistently infected mice strongly express neutralizing antibodies (Table 1). Furthermore, an abundance of background information is available on experimental laboratory mice. Therefore, the experimental mouse model is useful for detailed analyses, particularly immunological characterization. In this study, we followed the status of persistently infected mice and analyzed their offspring for potential vertical transmission of HTNV infection.

Pregnant BALB/c/Slc mice and Slc:ICR mice were obtained from SLC (Hamamatsu, Japan). All animal experiments in this study were carried out under the guidance of the Hokkaido University Animal Research Committee and in accordance with their guidelines, performed in a BSL3 facility. For the production of persistently infected mice, BALB/c mice were subcutaneously inoculated with 1.3 focus-forming units (FFU) of HTNV strain 76-118 within 24 h of birth [1.3 FFU = 0.1 $NMLD_{50}$ (50% newborn mouse lethal dose)]. A total of 17 mice were examined at 1–12 weeks after infection. The antibody response in these animals was evaluated, as shown in Table 1. High HTNV-specific IgG antibody titers (titers $\geq$ 5,120) were observed at 4, 8, and 12 weeks after infection. The IgG antibodies were detected even at 23 weeks after infection (data not shown). Similarly, IgM antibodies (titer: 80–320) were continuously observed at least until 12 weeks post-infection. Neutralizing antibodies (titer: 320–640) were also observed in all animals at all investigated time points. In addition, virus was isolated from the brains or lungs of the mice until 12 weeks post-infection, although the isolation rate decreased slightly. Viral antigen in the lung started to disappear gradually from 8 to 15 weeks post-infection and completely disappeared 20 weeks post-infection (data not shown). The disappearance of viral antigen seemed to be correlated with a reduced viral load that is reflected in an increasing number of negatives in the bioassay used (Table 1). In contrast, adult mice that were intraperitoneally inoculated with 10^5 FFU of HTNV for the production of transiently infected mice showed HTNV-specific IgM antibodies only 1 week after infection (titer: 160–320, $n = 6$ mice), and the titer quickly dropped within 3 weeks after infection (titer: <40, $n = 6$). The titers of HTNV-specific IgG antibodies increased until 3 weeks after infection in these transiently infected mice (Table 1) and, usually, neutralizing antibodies also increased until 3 weeks after infection [2, 21].

Recently, we reported that in the persistent infection model, mice had a reduced number of virus-specific CTLs in their spleen, so that viral elimination was delayed [20]. It has been reported that CTLs are regulated by other immune cells, for example dendritic cells, or inflammatory

Table 1 Analysis of mice immunized with a sublethal dose of HTNV by IFA and FRNT, and virus isolation

Weeks after infection	No.	IFA titers[a]		FRNT titers[b]	Bioassay[c]	
		IgG	IgM		Brain	Lung
New born 1 week	1	<40	80	NT	NT	NT
	2	<40	160	NT	NT	NT
New born 4 weeks	1	10,240	160	640	+	+
	2	5,120	160	640	+	+
	3	5,120	80	320	−	+
	4	5,120	160	640	+	+
	5	5,120	160	320	−	−
	6	5,120	160	640	−	+
New born 8 weeks	1	10,240	160	320	+	+
	2	10,240	160	320	−	+
	3	5,120	320	640	−	−
	4	10,240	320	640	−	+
	5	20,480	320	320	+	+
New born 12 weeks	1	10,240	160	640	−	−
	2	10,240	320	320	−	−
	3	10,240	160	640	+	+
	4	10,240	160	320	−	+
Adult 1 week	1	80	320			
	2	80	160			
	3	80	160			
	4	160	320			
	5	80	160			
	6	80	160			
Adult 3 weeks	1	640	<40			
	2	640	<40			
	3	5,120	<40			
	4	640	<40			
	5	640	<40			
	6	320	<40			

Seventeen newborn mice (within 24 h after birth) and twelve 5-week-old mice were inoculated with HTNV. They were sacrificed at various time points

NT not tested

[a] Indirect immunofluorescent antibody (IFA) tests were performed using acetone-fixed smears of Vero E6 cells infected with HTNV 76-118 as antigen. Fluorescein isothiocyanate (FITC)-conjugated goat anti-mouse IgG [IgA + IgG + IgM(H + L)] or anti-mouse IgM (Zymed Laboratories, San Francisco, CA, USA) was used as a secondary antibody. The IFA titers are expressed as the reciprocal of the highest dilution of antiserum that resulted in specific fluorescence

[b] FRNT was performed as described previously [1]. The neutralizing antibody titer was defined as the highest serum dilution that resulted in greater than 80% reduction in the number of infected cell foci

[c] The brains and lungs were removed from HTNV-infected mice. Groups of two or three newborn ICR mice were inoculated subcutaneously with 50 µl of the homogenates. The presence of the virus was assessed by seroconversion of the mice at 4 weeks after inoculation

+, all newborn ICR mouse sera were positive for HTNV. −, all newborn ICR mouse sera were negative for HTNV

cytokines after infection [11]. We suspected such a reduction in CTLs in persistent hantavirus infection in mice was also involved in these immune cells. Therefore, we have examined the infectivity to such as immune cells in spleen by histological study. Mice were anesthetized and perfused intracardially with 4% paraformaldehyde (PFA) in phosphate buffer (PB, pH 7.4), followed by brief perfusions with sucrose [13]. The spleens and lungs were stained with the Alexa Fluor 488-labeled monoclonal antibody (MAb) E5/G6 [18]. Nuclear staining was achieved using TOTO3 (Molecular Probes). Images were obtained by confocal microscopy (FLUOVIEW FV1000; Olympus, Japan). We detected N antigen in lung and spleen tissue at 2 weeks after infection in this persistent infection model. We detected high levels of N antigen in the intra-alveolar septum region (Fig. 1a), alveolar macrophages (Fig. 1b), and the elastic fiber region (Fig. 1c) of the lungs at 2 weeks after infection. Even though most of the antigen had disappeared at 8 weeks after infection, antigen remained in the intra-alveolar septum region of the lungs (data not shown). We detected N-antigen-positive cells in the marginal zone of each spleen (Fig. 1d). Generally, immune cells are distributed in the spleen marginal zone after pathogen invasion. Therefore, we have to identify N-positive cells to know whether these cells were involved in the regulation of CTLs in persistently infected mice.

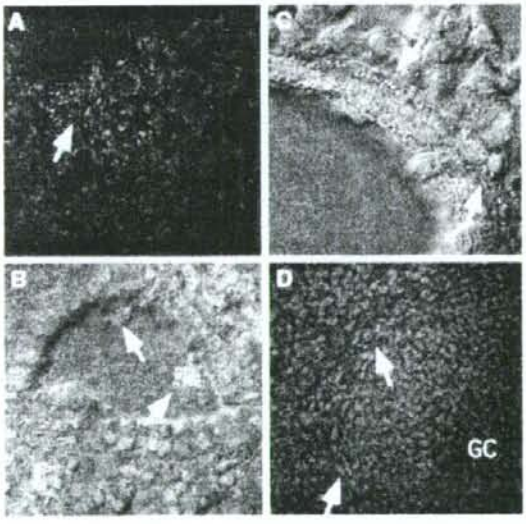

Fig. 1 Immunohistochemical analysis of persistently infected mice. Persistently infected mice were sacrificed 2 weeks after infection. The lungs and spleen were removed, fixed, sectioned, and stained with E5G6 antibody (*green*) and TOTO3 (*red*). **a** N-positive cells are observed in the intra-alveolar septum region of the lung. **b** Infected alveolar macrophages are observed in the lung. **c** Clustered N antigen is detected in the elastic fibers of the bronchiole. **d** N-positive cells are shown localized in the marginal zone of the spleen. Magnification: **a** ×20, **b** ×60, **c** ×180, **d** ×60

Finally, to examine the possibility of vertical transmission from persistently infected mice to their progeny, three pairs of these mice were mated, the offspring and dams were sacrificed at various time points (Fig. 2a), and tissues were examined by Western blotting and RT-PCR. We detected hantavirus N antigen and RNA in the dams' lungs (12 weeks old, $n = 2$); however, no antigen or RNA was detected in their progeny (10 days old; Fig. 2b, c, 4 weeks old; data not shown, $n = 6$). Although a high level of IgG antibody [immunofluorescent antibody (IFA) titer: 5,120] was observed until 28 days after birth and the mice maintained low IgG antibody levels until 90 days (data not shown), we could not observe IgM antibody in the infants (10 days old, 4 weeks old) even though their dams (12 weeks old, $n = 2$) had IgM antibody (Fig. 2d, data not shown). This indicates that the HTNV-specific IgG antibodies were maternally derived. To confirm a lack of infection in the infants derived from and nursed by the persistently infected dams, we used FACS analysis to prove the presence of HTNV-specific $CD8^+$ T cells. We used flow cytometry to assay the cytokines produced by $CD8^+$ T cells incubated with HTNV-infected antigen-presenting cells [20]. Antigen-negative 3-week-old (progeny 1,2) and 20-week-old (progeny 3,4) offspring from a 17-week-old HTNV-antigen-positive persistently infected dam were analyzed. No HTNV-specific IFN-γ^+ $CD8^+$ T cells were found in any of the progeny (Fig. 2e), suggesting that none of the offspring had ever been infected with HTNV. These data are in agreement with those from previous rodent studies [8, 14, 17].

The transfer of maternal antibodies from mother to progeny is well known in avian and mammalian species and is believed to protect the newborn against pathogens in the environment. Several reports have described this phenomenon for hantavirus infection [8, 14, 23]; however, there is a scarcity of studies examining the vertical transmission of hantaviruses in wild-living rodents that are persistently infected [15, 17]. To examine vertical transmission from persistently infected dams to their progeny, we studied the progeny of persistently HTNV-infected mice by Western blotting, RT-PCR, FACS analysis, and IFA. The progeny had no HTNV-antigen in their lungs, no virus-specific CTLs, and no anti-HTNV IgM antibodies, although they maintained anti-HTNV IgG antibodies until 90 days after birth. These results indicate that the progeny of persistently infected laboratory mice are immune to HTNV and that vertical transmission of HTNV from persistently infected dams to their offspring does not occur. Thus, these results suggest that the virus is transmitted horizontally in nature, from rodent to rodent, and several reports have suggested that a high dose is required for

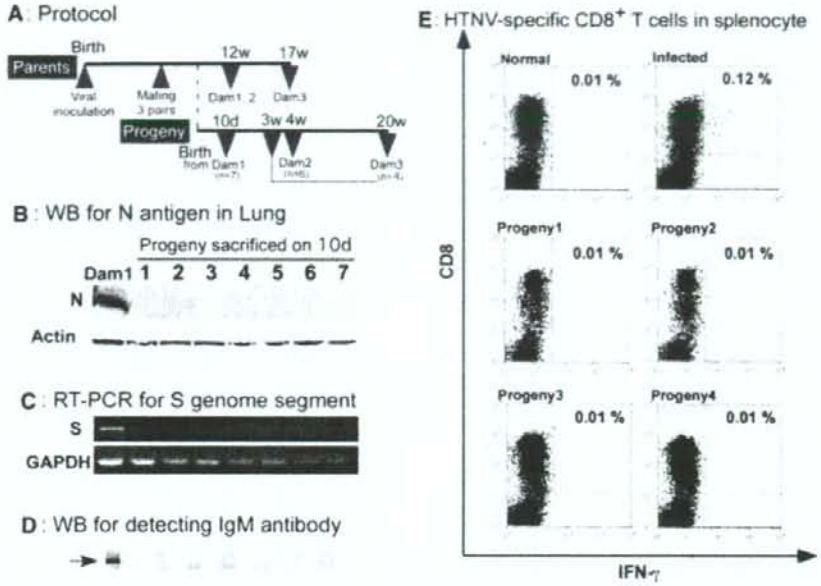

Fig. 2 Analysis of progeny from persistently infected mice. Dam1 possessed both N antigen and viral genomic RNA in lung, and its seven progenies lacked both viral antigen and RNA in lung. The same results were obtained from *dam2* and *dam3* and their six or four progenies (data not shown). **a** Experimental protocol. Three pairs of BALB/c parents were mated and analyzed at the time point indicated in *lane 1*; their newborns were analyzed at the time point indicated in *lane 2*. **b** Western blot (*WB*) analysis of lung lysates from persistently HNTV-infected mice and their newborn offspring [3]. The MAbs E5/G6 and ECO2 were used to detect the membrane-bound antigens [22]. Horseradish peroxidase (*HRP*)-conjugated goat anti-mouse IgG (Zymed Laboratories) was used as a secondary antibody. Actin, the control protein, was detected using mouse anti-β actin antibody (Sigma). **c** RT-PCR analysis of lungs from HNTV-infected mice and their newborn offspring to detect trace amounts of virus RNA. Lungs were homogenized and isolated by ISOGEN (NIPPON GENE). The isolated RNA was reverse transcribed using random hexamer and SuperScript II (Invitrogen). Each cDNA was amplified with hantavirus-specific primers MurS110F [5′CAGAAGGTIAIGGATG CAGA3′] and MurS1160R [5′TGGTCCAGTTGTATRCCCAT3′] or control GAPDH primers [5′TGCACCACCAACTGCTTAG3′, 5′GG ATGCAGGGATGATGTTC3′]. **d** Detection of IgM antibodies by WB. Recombinant HTNV N derived from high five cells was used [1]. Sera from the progeny and their persistently infected dam were used at a 1:10 dilution. Secondary antibody is HRP-anti-mouse IgM (Zymed Laboratories, San Francisco, CA, USA). **e** Immune responses of IFN-γ-producing HTNV-specific $CD8^+$ T cells in progeny (from *dam3*). Spleen cells were cultured with HTNV-infected P388D1 cells. The cells were stained with ethidium monoazide bromide (*EMA*) (Invitrogen), anti-CD8a PE (Ly-2) antibodies (eBioscience, San Diego, CA, USA), and FITC-conjugated rat anti-mouse gamma interferon (IFN-γ) antibody (Caltag Laboratories, San Francisco, CA). IFN-γ^+ cells were analyzed by flow cytometry using a FACS Calibur (Becton Dickinson, Franklin Lakes, NJ, USA) with the gates set for EMA-negative cells. The data were analyzed using FlowJo software (Tree Star, San Carlos, CA, USA). "*Infected*" indicates that the adult BALB/c mouse inoculated with HTNV recovered (positive control). "*Normal*" denotes a normal BALB/c mouse (negative control)

horizontal transmission between rodents in experimentally persistently infected animals [9, 15]. Efficient transmission may depend on the immune status influenced by infections with other pathogens of a different nature. Here, we found that vertical transmission from persistently infected laboratory mice does not occur. To prove the absence of vertical transmission of hantaviruses, further studies should be dedicated to the influence of the load and tissue distribution of hantavirus in persistently infected dams of laboratory mice and natural rodent hosts.

Acknowledgments We thank Dr. H. Sawa and Dr. T. Kimura for their assistance with the confocal immunofluorescence microscope and cryostat. Takako Shibuya is thanked for technical help. This work was supported in part by a grant from the 21st Century COE Program of Excellence for Zoonosis Control and in part by Grants-in-Aid for Scientific Research and the Development of Science from the Ministry of Education, Culture, Sports, Science, and Technology, Japan.

References

1. Araki K, Yoshimatsu K, Ogino M, Ebihara H, Lundkvist A, Kariwa H, Takashima I, Arikawa J (2001) Truncated hantavirus nucleocapsid proteins for serotyping Hantaan, Seoul, and Dobrava hantavirus infections. J Clin Microbiol 39:2397–2404
2. Araki K, Yoshimatsu K, Lee BH, Kariwa H, Takashima I, Arikawa J (2003) Hantavirus-specific CD8(+)-T-cell responses in newborn mice persistently infected with Hantaan virus. J Virol 77:8408–8417
3. Araki K, Yoshimatsu K, Lee BH, Okumura M, Kariwa H, Takashima I, Arikawa J (2004) Age-dependent hantavirus-specific

CD8(+) T-cell responses in mice infected with Hantaan virus. Arch Virol 149:1373–1382
4. Arikawa J, Ito M, Yao JS, Kariwa H, Takashima I, Hashimoto N (1994) Epizootiological studies of hantavirus infection among urban rats in Hokkaido, Japan: evidences for the persistent infection from the sero-epizootiological surveys and antigenic characterizations of hantavirus isolates. J Vet Med Sci 56:27–32
5. Botten J, Mirowsky K, Kusewitt D, Ye C, Gottlieb K, Prescott J, Hjelle B (2003) Persistent Sin Nombre virus infection in the deer mouse (*Peromyscus maniculatus*) model: sites of replication and strand-specific expression. J Virol 77:1540–1550
6. Childs JE, Ksiazek TG, Spiropoulou CF, Krebs JW, Morzunov S, Maupin GO, Gage KL, Rollin PE, Sarisky J, Enscore RE et al (1994) Serologic and genetic identification of *Peromyscus maniculatus* as the primary rodent reservoir for a new hantavirus in the southwestern United States. J Infect Dis 169:1271–1280
7. Compton SR, Jacoby RO, Paturzo FX, Smith AL (2004) Persistent Seoul virus infection in Lewis rats. Arch Virol 149:1325–1339
8. Dohmae K, Koshimizu U, Nishimune Y (1993) In utero and mammary transfer of hantavirus antibody from dams to infant rats. Lab Anim Sci 43:557–561
9. Dohmae K, Okabe M, Nishimune Y (1994) Experimental transmission of hantavirus infection in laboratory rats. J Infect Dis 170:1589–1592
10. Dohmae K, Nishimune Y (1995) Protection against hantavirus infection by dam's immunity transferred vertically to neonates. Arch Virol 140:165–172
11. Harty JT, Badovinac VP (2008) Shaping and reshaping $CD8^+$ T-cell memory. Nat Rev Immunol 8:107–119
12. Hutchinson KL, Rollin PE, Peters CJ (1998) Pathogenesis of a North American hantavirus, Black Creek Canal virus, in experimentally infected *Sigmodon hispidus*. Am J Trop Med Hyg 59:58–65
13. Ikegami K, Heier RL, Taruishi M, Takagi H, Mukai M, Shimma S, Taira S, Hatanaka K, Morone N, Yao I, Campbell PK, Yuasa S, Janke C, Macgregor GR, Setou M (2007) Loss of alpha-tubulin polyglutamylation in ROSA22 mice is associated with abnormal targeting of KIF1A and modulated synaptic function. Proc Natl Acad Sci USA 104:3213–3218
14. Kallio ER, Poikonen A, Vaheri A, Vapalahti O, Henttonen H, Koskela E, Mappes T (2006) Maternal antibodies postpone hantavirus infection and enhance individual breeding success. Proc Biol Sci 273:2771–2776
15. Lee HW, Lee PW, Baek LJ, Song CK, Seong IW (1981) Intraspecific transmission of Hantaan virus, etiologic agent of Korean hemorrhagic fever, in the rodent *Apodemus agrarius*. Am J Trop Med Hyg 30:1106–1112
16. Meyer BJ, Schmaljohn CS (2000) Persistent hantavirus infections: characteristics and mechanisms. Trends Microbiol 8:61–67
17. Morita C, Morikawa S, Sugiyama K, Komatsu T, Ueno H, Kitamura T (1993) Inability of a strain of Seoul virus to transmit itself vertically in rats. Jpn J Med Sci Biol 46:215–219
18. Okumura M, Yoshimatsu K, Araki K, Lee BH, Asano A, Agui T, Arikawa J (2004) Epitope analysis of monoclonal antibody E5/G6, which binds to a linear epitope in the nucleocapsid protein of hantaviruses. Arch Virol 149:2427–2434
19. Tanishita O, Takahashi Y, Okuno Y, Tamura M, Asada H, Dantas JR Jr, Yamanouchi T, Domae K, Kurata T, Yamanishi K (1986) Persistent infection of rats with haemorrhagic fever with renal syndrome virus and their antibody responses. J Gen Virol 67(Pt 12):2819–2824
20. Taruishi M, Yoshimatsu K, Araki K, Okumura M, Nakamura I, Kajino K, Arikawa J (2007) Analysis of the immune response of Hantaan virus nucleocapsid protein-specific $CD8^+$ T cells in mice. Virology 365:292–301
21. Yoshimatsu K, Yoo YC, Yoshida R, Ishihara C, Azuma I, Arikawa J (1993) Protective immunity of Hantaan virus nucleocapsid and envelope protein studied using baculovirus-expressed proteins. Arch Virol 130:365–376
22. Yoshimatsu K, Arikawa J, Tamura M, Yoshida R, Lundkvist A, Niklasson B, Kariwa H, Azuma I (1996) Characterization of the nucleocapsid protein of Hantaan virus strain 76-118 using monoclonal antibodies. J Gen Virol 77(Pt 4):695–704
23. Zhang XK, Takashima I, Hashimoto N (1988) Role of maternal antibody in protection from hemorrhagic fever with renal syndrome virus infection in rats. Arch Virol 103:253–265

Molecular phylogeny of a newfound hantavirus in the Japanese shrew mole (*Urotrichus talpoides*)

Satoru Arai*, Satoshi D. Ohdachi†, Mitsuhiko Asakawa‡, Hae Ji Kang§, Gabor Mocz¶, Jiro Arikawa‖, Nobuhiko Okabe*, and Richard Yanagihara§**

*Infectious Disease Surveillance Center, National Institute of Infectious Diseases, Tokyo 162-8640, Japan; †Institute of Low Temperature Science, Hokkaido University, Sapporo 060-0819, Japan; ‡School of Veterinary Medicine, Rakuno Gakuen University, Ebetsu 069-8501, Japan; §John A. Burns School of Medicine, University of Hawaii at Manoa, Honolulu, HI 96813; ¶Pacific Biosciences Research Center, University of Hawaii at Manoa, Honolulu, HI 96822; and ‖Institute for Animal Experimentation, Hokkaido University, Sapporo 060-8638, Japan

Communicated by Ralph M. Garruto, Binghamton University, Binghamton, NY, September 10, 2008 (received for review August 8, 2008)

Recent molecular evidence of genetically distinct hantaviruses in shrews, captured in widely separated geographical regions, corroborates decades-old reports of hantavirus antigens in shrew tissues. Apart from challenging the conventional view that rodents are the principal reservoir hosts, the recently identified soricid-borne hantaviruses raise the possibility that other soricomorphs, notably talpids, similarly harbor hantaviruses. In analyzing RNA extracts from lung tissues of the Japanese shrew mole (*Urotrichus talpoides*), captured in Japan between February and April 2008, a hantavirus genome, designated Asama virus (ASAV), was detected by RT-PCR. Pairwise alignment and comparison of the S-, M-, and L-segment nucleotide and amino acid sequences indicated that ASAV was genetically more similar to hantaviruses harbored by shrews than by rodents. However, the predicted secondary structure of the ASAV nucleocapsid protein was similar to that of rodent- and shrew-borne hantaviruses, exhibiting the same coiled-coil helix at the amino terminus. Phylogenetic analyses, using the maximum-likelihood method and other algorithms, consistently placed ASAV with recently identified soricine shrew-borne hantaviruses, suggesting a possible host-switching event in the distant past. The discovery of a mole-borne hantavirus enlarges our concepts about the complex evolutionary history of hantaviruses.

host switching | talpid | evolution | Japan

Dating from investigations conducted independently by Japanese and Russian medical scientists along opposite sides of the Amur River in the 1930s and 1940s, rodents have been suspected to harbor the etiological agent(s) of hemorrhagic fever with renal syndrome (HFRS) (1, 2). After a several decades-long impasse, the striped field mouse (*Apodemus agrarius*) was identified as the reservoir host of Hantaan virus (3), the prototype virus of HFRS (4). This seminal discovery made possible the identification of genetically distinct hantaviruses in other murinae and arvicolinae rodent species (5–12). Also, a previously unrecognized, frequently fatal respiratory disease, called hantavirus pulmonary syndrome (HPS) (13), is now known to be caused by hantaviruses harbored by neotominae and sigmodontinae rodents in the Americas, the prototype being Sin Nombre virus (SNV) in the deer mouse (*Peromyscus maniculatus*) (14). Remarkably, each of these hantaviruses appears to share a long coevolutionary history with a specific rodent host species. That is, based on phylogenetic analyses of full-length viral genomic and rodent mitochondrial DNA (mtDNA) sequences, these hantaviruses segregate into clades, which parallel the evolution of rodents in the murinae, arvicolinae, neotominae, and sigmodontinae subfamilies (15, 16).

Until recently, the single exception to the strict rodent association of hantaviruses was Thottapalayam virus (TPMV), a long-unclassified virus originally isolated from the Asian house shrew (*Suncus murinus*) (17, 18). Analysis of the recently acquired full genome of TPMV strongly supports an ancient non-rodent host origin and an early evolutionary divergence from rodent-borne hantaviruses (19, 20). Employing RT-PCR and oligonucleotide primers based on the TPMV genome, we have targeted the discovery of hantaviruses in shrew species from widely separated geographical regions, including the Chinese mole shrew (*Anourosorex squamipes*) from Vietnam (21), Eurasian common shrew (*Sorex araneus*) from Switzerland (22), northern short-tailed shrew (*Blarina brevicauda*), masked shrew (*Sorex cinereus*), and dusky shrew (*Sorex monticolus*) from the United States (23, 24) and Ussuri white-toothed shrew (*Crocidura lasiura*) from Korea (J.-W. Song and R. Yanagihara, unpublished observations). Many more shrew-hantavirus associations undoubtedly exist, as evidenced by preliminary studies of *Sorex caecutiens* and *Sorex roboratus* from Russia (H. J. Kang, S. Arai and R. Yanagihara, unpublished observations) and *Sorex palustris*, *Sorex trowbridgii*, and *Sorex vagrans* from North America (H. J. Kang and R. Yanagihara, unpublished observations).

In addition to challenging the view that rodents are the sole or principal reservoirs of hantaviruses, the discovery of soricid-borne hantaviruses predicts that other soricomorphs, notably talpids, might also harbor genetically distinct hantaviruses. In this regard, hantavirus antigens have been detected by enzyme immunoassay and fluorescence techniques in tissues of the European common mole (*Talpa europea*) captured in Russia (25) and Belgium (26), but no reports are available about hantavirus infection in shrew moles. Relying on oligonucleotide primers designed from our expanding sequence database of shrew-borne hantaviruses, we have identified a hantavirus genome, designated Asama virus (ASAV), in the Japanese shrew mole (*Urotrichus talpoides*). Genetic and phylogenetic analyses indicate that ASAV is distinct but related to hantaviruses harbored by Old World soricine shrews, suggesting a very ancient evolutionary history, probably involving multiple host-switching events in the distant past.

Results

RT-PCR Detection of Hantavirus Sequences. In using RT-PCR to analyze RNA extracts, from lung tissues of three Laxmann's shrew (*Sorex caecutiens*), five slender shrew (*Sorex gracillimus*), six long-clawed shrew (*Sorex unguiculatus*), one dsinezumi shrew (*Crocidura dsinezumi*), and six Japanese shrew mole (*Urotrichus talpoides*), hantavirus sequences were not detected in shrew tissues, but were found in one of two and in two of three Japanese shrew moles (Fig. 1), captured in Ohtani (34 28′14.0″ N; 136 45′46.2″ E) and near

Author contributions: S.A. and R.Y. designed research; S.A., S.D.O., M.A., J.A., N.O., and R.Y. performed research; S.A. and H.J.K. contributed new reagents/analytic tools; S.A., S.D.O., H.J.K., G.M., and R.Y. analyzed data; and S.A., G.M., J.A., and R.Y. wrote the paper.

The authors declare no conflict of interest.

Freely available online through the PNAS open access option.

Data deposition: The sequences reported in this paper have been deposited in the GenBank database [accession numbers: ASAV S segment (EU929070, EU929071, EU929072); ASAV M segment (EU929073, EU929074, EU929075); and ASAV L segment (EU929076, EU929077, EU929078).

**To whom correspondence should be addressed at: John A. Burns School of Medicine, University of Hawaii at Manoa, 651 Ilalo Street, BSB 320L, Honolulu, HI 96813. E-mail: yanagiha@pbrc.hawaii.edu.

Fig. 1. Japanese shrew mole (*Urotrichus talpoides*) (family *Talpidae*, subfamily Talpinae), one of two endemic shrew mole species found only in Japan.

Asama River (34°28′12.79″ N; 136°45′45.81″ E), respectively, located approximately 1 km apart at an elevation of 50 m in Mie Prefecture, during February and April 2008. After the initial detection of hantavirus sequences, amplification of the S-, M-, and L-genomic segments was accomplished by using oligonucleotide primers based on conserved regions.

Nucleotide and Amino Acid Sequence Analysis. The S, M, and L segments of ASAV, as amplified from tissues of three wild-caught Japanese shrew moles, indicated an overall genomic structure similar to that of other rodent- and soricid-borne hantaviruses. The nucleotide and deduced-amino acid sequences of each ASAV genomic segment were highly divergent from that of rodent-borne hantaviruses, differing by approximately 30–40% (Table 1).

The S-genomic segment of ASAV (1,801 nucleotides for strains H4 and N9 and 1,756-nucleotides for strain N10) encoded a predicted nucleocapsid (N) protein of 434 amino acids, starting at nucleotide position 39, and a 3′-noncoding region (NCR) of approximately 465 nucleotides. The hypothetical NSs opening reading frame, typically found in the S segment of arvicolinae, neotominae, and sigmodontinae rodent-borne hantaviruses, was not found in ASAV. The interstrain variation of the S segment among the ASAV strains was negligible (1.1% at the nucleotide and 0% at the amino acid levels). In the hypervariable region of the N protein, between amino acid residues 244 and 269, ASAV differed by 18–20 and 20–22 amino acid from soricine shrew- and rodent-borne hantaviruses, respectively. Sequence similarity of the entire S-genomic segment of ASAV strains H4, N9, and N10 was higher with soricine shrew-borne hantaviruses than with hantaviruses harbored by rodents (Table 1).

Table 1. Nucleotide and amino acid sequence similarity (%) between ASAV strain N10 and representative rodent- and shrew-borne hantaviruses

	S segment		M segment		L segment	
Virus strain	1710 nt	434 aa	3604 nt	1141 aa	6126 nt	2041aa
HTNV 76–118	58.5	62.7	62.7	59.4	70.3	74.6
SEOV 80–39	63.1	62.0	62.8	59.1	70.4	74.7
SOOV SOO-1	62.8	62.9	63.3	59.7	70.2	74.3
DOBV Greece	62.2	62.2	63.0	59.3	70.2	75.7
PUUV Sotkamo	59.3	59.3	59.6	52.2	68.1	68.0
TULV 5302v	61.5	59.4	60.5	52.6	68.3	67.9
PHV PH-1	60.7	59.3	59.3	51.9	66.4	67.1
SNV NMH10	60.9	58.9	59.0	54.1	68.2	68.8
RPLV MSB89866	—	—	68.8	63.5	75.2	83.2
CBNV CBN-3	67.7	70.4	68.2	71.0	76.0	84.7
ARRV MSB73418	65.7	66.6	70.9	77.0	73.8	83.5
JMSV MSB89332	66.2	66.9	—	—	74.3	82.6
SWSV mp70	63.8	69.9	75.2	79.5	75.0	83.2
ASAV H4	98.9	100	99.3	99.6	98.2	99.6
ASAV N9	100	100	99.9	100	100	100
MJNV 05–11	57.2	46.0	56.1	44.4	65.8	61.5
TPMV VRC	58.0	45.8	57.7	43.0	64.3	62.0

Abbreviations: ARRV, Ash River virus; ASAV, Asama virus; CBNV, Cao Bang virus; DOBV, Dobrava virus; HTNV, Hantaan virus; JMSV, Jemez Spring virus; MJNV, Imjin virus; PHV, Prospect Hill virus; PUUV, Puumala virus; RPLV, Camp Ripley virus; SEOV, Seoul virus; SNV, Sin Nombre virus; SOOV, Soochong virus; SWSV, Seewis virus; TPMV, Thottapalayam virus; TULV, Tula virus. nt, nucleotides; aa, amino acids.

The 3,646-nucleotide full-length M-genomic segment of ASAV encoded a predicted glycoprotein of 1,141 amino acids, starting at nucleotide position 41, and a 183-nucleotide 3′-NCR. Four potential N-linked glycosylation sites (three in Gn at amino acid positions 138, 352, 404, and one in Gc at position 933) were found in ASAV. In addition, the highly conserved WAASA amino acid motif, which in ASAV was WAVSA (amino acid positions 649–653), was present. An interstrain variation of 0.1–0.7% and 0–0.4% at the nucleotide and amino acid levels, respectively, was found among ASAV strains H4, N9, and N10. The full-length Gn/Gc amino acid sequence of ASAV exhibited the highest similarity with Seewis virus (79.5%) from the Eurasian common shrew (Table 1).

Analysis of the nearly full-length 6,126-nucleotide (2,041-amino acid) L segment of ASAV revealed the five conserved motifs (A–E), identified among all hantavirus RNA polymerases. The overall high sequence similarity of the L segment among ASAV and rodent- and soricid-borne hantaviruses was consistent with the functional constraints on the RNA-dependent RNA polymerase (Table 1).

Secondary Structure of N Protein. Secondary structure analysis revealed striking similarities, as well as marked differences, among the N protein sequences of ASAV and 13 representative rodent- and soricid-hantaviruses. Each sequence appeared to adopt a two-domain, predominantly α-helical structure joined by a central β-pleated sheet. Whereas the length of the N-terminal domain was mostly invariant, the length of the central β-pleated sheet and of the adjoining C-terminal α-helical domain showed systematic reciprocal structural changes according to the genetic relationship and evolutionary descent of the individual sequences.

The N-terminal α-helical domain, from residues 1 to approximately 140, was composed of four helices connected by large loops (representative viruses shown in Fig. 2). The C-terminal α-helical domain, from residues 210/230 to 430, contained seven to nine helices that were connected by tighter loops (Fig. 2). And the central β-pleated region, from residues 140 to 210/230, was composed of three to five possible anti-parallel strands. Interestingly, an increasing number of strands in this section were observed when the hantaviral sequences were arranged according to their positions in the phylogenetic tree. This resulted in a widening of the central β-pleated region with a concomitant shortening of the C-terminal α-helical domain while preserving the total length of the protein. The helix adjoining the central β-sheet progressively shortened in this architectural change. These structural alterations were reversed in TPMV, which was evolutionarily more distant from the other sequences (Fig. 2).

Phylogenetic Analysis. Exhaustive phylogenetic analyses based on nucleotide and deduced amino acid sequences of the S-, M-, and L-genomic segments, generated by the maximum-likelihood (ML) method, indicated that ASAV was distinct from rodent-borne hantaviruses (with high posterior node probabilities based on 30,000 trees) (Fig. 3). Nearly identical topologies were consistently derived, by using various algorithms and different taxa and combinations of taxa, suggesting an ancient evolutionary origin. The most strikingly consistent feature was the phylogenetic position of ASAV with soricine shrew-borne hantaviruses, rather than being placed as an outgroup beyond TPMV, the prototype crocidurine shrew-borne hantavirus. That is, the prediction that a shrew mole-associated hantavirus would be phylogenetically distant from hantaviruses harbored by shrews was not validated.

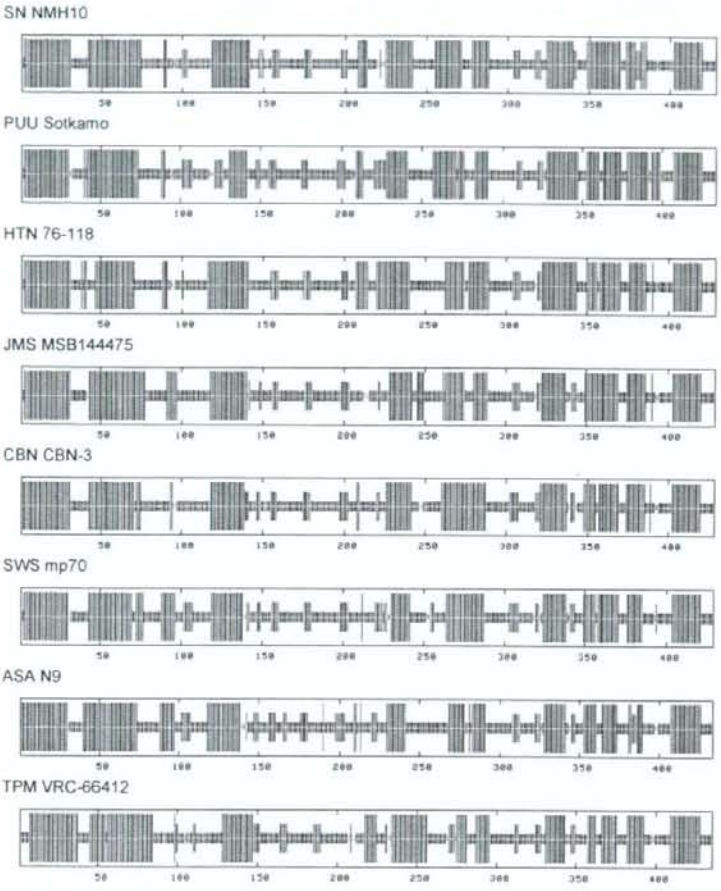

Fig. 2. Consensus secondary structure of N protein of ASAV and representative rodent- and soricid-borne hantaviruses, predicted using a high-performance method implemented on the NPS@ structure server (47). As shown, the ASAV N protein was very similar to that of other hantaviruses, characterized by the same coiled-coil helix at the amino terminal end and similar secondary structure motifs at their carboxyl terminals. The predicted structures were represented by colored bars to visualize the schematic architecture: α-helix, blue; β-sheet, red; coil, magenta; unclassified, gray. For simplicity, turns and other less frequently occurring secondary structural elements were omitted. All sequences are numbered from Met-1.

Sequence and Phylogenetic Analysis of Mole mtDNA. Molecular confirmation of the taxonomic identification of the hantavirus-infected Japanese shrew moles based on morphological features was achieved by amplification and sequencing of the 1,140-nucleotide mtDNA cytochrome *b* gene. Phylogenetic analysis showed distinct grouping of hantavirus-infected *U. talpoides* from this study with other *U. talpoides* mtDNA sequences available in GenBank, rather than with soricids or rodents (Fig. 4).

Discussion

Newfound Shrew Mole-Borne Hantavirus. Despite reports of hantavirus antigens in tissues of the Eurasian common shrew (*Sorex araneus*), alpine shrew (*Sorex alpinus*), Eurasian water shrew (*Neomys fodiens*), and common mole (*Talpa europea*) (25–28), shrews and moles have been generally dismissed as being unimportant in the transmission dynamics of hantaviruses. With the recent demonstration that TPMV and other newly identified soricid-borne hantaviruses are genetically distinct and phylogenetically distant from rodent-borne hantaviruses (19–24), the conventional view that rodents are the principal or primordial reservoir hosts of hantaviruses is being challenged. In its wake, a compelling conceptual framework, or paradigm shift, is emerging that supports an ancient origin of hantaviruses in soricomorphs (or insectivores). To this emerging concept must now be added the first molecular evidence of a newfound hantavirus, designated ASAV, in the Japanese shrew mole (family *Talpidae*, subfamily *Talpinae*). The demonstration of ASAV sequences in this endemic shrew mole species captured at different times and in two separate locations in Mie Prefecture argues strongly against this being an isolated or coincidental event. Instead, these data suggest a well established coexistence of this newfound hantavirus in the Japanese shrew mole and further solidifies the notion of a long-standing evolutionary association between soricomorphs and hantaviruses.

Shrew moles differ from typical or true moles in that they look like shrews and are much less specialized for burrowing. The greater Japanese shrew mole, which morphologically resembles semifossorial shrew moles in China (*Scaptonyx*) and North America (*Neurotrichus*), is widely distributed in the lowlands and peripheral islands of Japan, except Hokkaido, and is not found on mainland Asia (29, 30). Also endemic in Japan, the lesser Japanese shrew mole (*Dymecodon pilirostris*) is largely restricted to mountainous regions on Honshu, Shikoku, and Kyushu and is considered the more ancestral species. As determined by cytochrome *b* mtDNA and nuclear recombination activating gene-1 (RAG1) sequence analyses, the greater and lesser Japanese shrew moles are closely related, but their evolutionary origins and biogeography remain unresolved (31, 32). The existence of two distinct chromosomal races of *U. talpoides*, geographically separated by the Fuji and Kurobe rivers in central Honshu (33, 34), provides an opportunity to further clarify the evolutionary origins of shrew mole-borne hantaviruses in Japan. Studies, now underway, will examine whether ASAV is harbored by *U. talpoides* in locations east of Mie

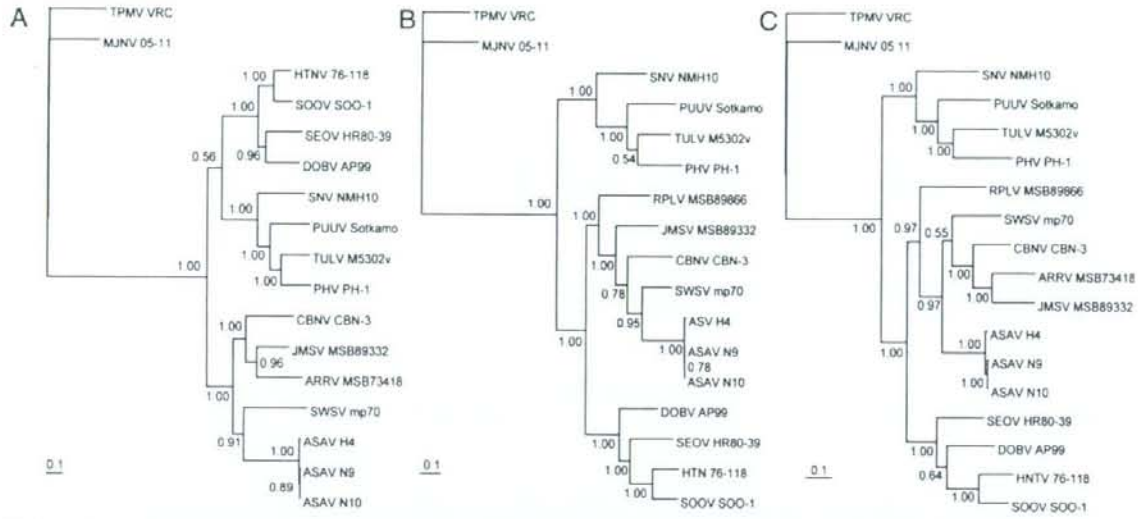

Fig. 3. Phylogenetic trees generated by the ML method, using the GTR+I+G model of evolution as estimated from the data, based on the alignment of the coding regions of the full-length (*A*) 1,302-nucleotide S and (*B*) 3,423-nucleotide M segments, and partial (*C*) 6,126-nucleotide L-genomic segment of ASAV. The phylogenetic positions of ASAV strains H4, N9, and N10 are shown in relationship to representative murinae rodent-borne hantaviruses, including Hantaan virus (HTNV 76–118, NC_005218, NC_005219, NC_005222), Soochong virus (SOOV SOO-1, AY675349, AY675353, DQ056292), Dobrava virus (DOBV AP99, NC_005233, NC_005234, NC_005235), and Seoul virus (SEOV HR80–39, NC_005236, NC_005237, NC_005238); arvicolinae rodent-borne hantaviruses, including Tula virus (TULV M5302v, NC_005227, NC_005228, NC_005226), Puumala virus (PUUV Sotkamo, NC_005224, NC_005223, NC_005225), and Prospect Hill virus (PHV PH-1, Z49098, X55129, EF646763); and a neotominae rodent-borne hantavirus, Sin Nombre virus (SNV NMH10, NC_005216, NC_005215, NC_005217). Also shown are Thottapalayam virus (TPMV VRC, AY526097, EU001329, EU001330) from the Asian house shrew (*Suncus murinus*); Imjin virus (MJNV 05–11, EF641804, EF641798, EF641806) from the Ussuri white-toothed shrew (*Crocidura lasiura*); Cao Bang virus (CBNV CBN-3, EF543524, EF543526, EF543525) from the Chinese mole shrew (*Anourosorex squamipes*); Ash River virus (ARRV MSB 73418, EF650086, EF619961) from the masked shrew (*Sorex cinereus*); Jemez Springs virus (JMSV MSB89332, EF619962, EF619960) from the dusky shrew (*Sorex monticolus*); and Seewis virus (SWSV mp70, EF636024, EF636025, EF636026) from the Eurasian common shrew (*Sorex araneus*). The numbers at each node are posterior node probabilities based on 30,000 trees: two replicate MCMC runs consisting of six chains of 3 million generations each sampled every 1,000 generations with a burn-in of 7,500 (25%). The scale bar indicates nucleotide substitutions per site. GenBank accession numbers: ASAV S segment (H4, EU929070; N9, EU929071; N10, EU929072); ASAV M segment (H4, EU929073; N9, EU929074; N10, EU929075); and ASAV L segment (H4, EU929076; N9, EU929077; N10, EU929078).

Prefecture, as well as ascertain whether *D. pilirostris* also serves as a reservoir of ASAV-related hantaviruses.

Although our RT-PCR attempts have failed to detect hantavirus sequences in other talpid species, including the long-nosed mole (*Euroscaptor longirostris*) (21) and eastern mole (*Scalopus aquaticus*) (H. J. Kang, J.-W. Song, and R. Yanagihara, unpublished observations), it may be because appropriate primers were not used. That is, based on the vast genetic diversity of soricid-borne hantaviruses, talpid-associated hantaviruses may be even more highly divergent and would require designing very different primers for amplification.

Finally, as for shrew-borne hantaviruses, the importance of this newfound shrew mole-associated hantavirus to human health warrants careful inquiry. Virus isolation attempts have been unsuccessful to date. In the meantime, an ASAV recombinant N protein is being prepared for use in enzyme immunoassays. In this regard, as evidenced by the corresponding sequence of YIEVNGIRKP in the ASAV N protein, the monoclonal antibody E5/G6, which recognizes the epitope YEDVNGIRKP (with variations) in rodent-borne hantaviruses (35), might be useful as a capturing antibody. In addition, other sensitive technologies, including nucleic acid and protein microarrays, are being developed to establish whether ASAV is pathogenic for humans.

Secondary Structure of Hantavirus N Protein. The overall N protein secondary structure of ASAV and other hantaviruses was compatible with a putative bilobed, three-dimensional protein architecture, which would allow the protein to clamp around the RNA as often observed in a variety of RNA-binding proteins. Whereas the core elements of the central β-pleated sheet appeared also to be conserved, more evolutionary variability was seen in the number of constituent strands and in the adjoining connecting elements and helices. This variability may reflect the function of this region as a flexible spacer element that can determine the relative orientation and separation of the two main α-helical domains and can accommodate the conformational changes upon RNA binding. The connecting regions could act as hinges of variable size leading to opening of the nucleocapsid. The flexible domain linkage would allow the interaction with the differently sized virus-specific RNA structures may modulate the oligomerization or assembly of the N protein in an evolutionarily and systematically changing fashion.

Phylogeny of Hantaviruses. Just as the identification of novel hantaviruses in the Therese shrew (*Crocidura theresae*) (36) and the northern short-tailed shrew (*Blarina brevicauda*) (23) heralded the discovery of other soricid-borne hantaviruses (21, 22, 24), the detection of ASAV in the Japanese shrew mole forecasts the existence of other hantaviruses in talpids. Perhaps more importantly, these findings emphasize that the evolutionary history and transmission dynamics of hantaviruses are far more rich and complex than originally imagined. That is, instead of a single progenitor virus being introduced into the rodent lineage more than 50 million years ago, mounting evidence supports a more ancient virus lineage with parallel coevolution of hantaviruses in crocidurine and soricine shrews. And given the sympatric and synchronistic coexistence of moles, shrews, and rodents, through a long continuum dating from the distant past to the present time, it seems

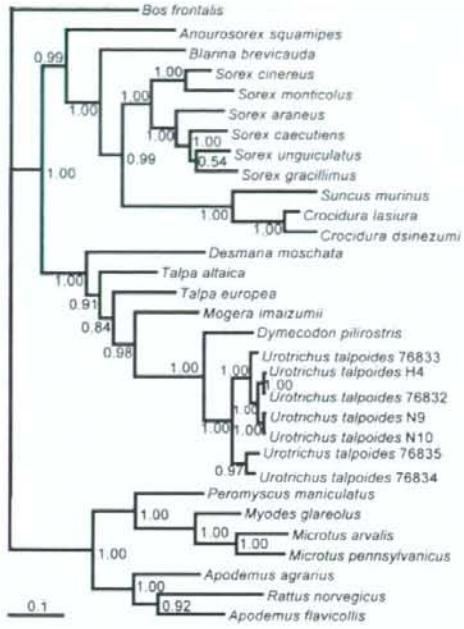

Fig. 4. Confirmation of host identification of ASAV-infected *Urotrichus talpoides* by mtDNA sequencing. Phylogenetic tree, based on the 1,140-nucleotide cytochrome *b* (cyt b) gene, was generated by the ML method. The phylogenetic positions of *Urotrichus talpoides* H4 (EU918369), N9 (EU918370), and N10 (EU918371) are shown in relationship to other *Urotrichus talpoides* cyt b sequences from GenBank (Ut76835: AB076835; Ut76834: AB076834; Ut76833: AB076833; Ut76832: AB076832), as well as other talpids, including *Desmana moschata* (AB076836), *Talpa altaica* (AB037602), *Talpa europea* (AB076829), *Mogera imaizumii* (AB037616), *Dymecodon pilirostris* (AB076830), and *Bos frontalis* (EF061237). Also shown are representative murinae rodents, including *Apodemus agrarius* (AB303226), *Apodemus flavicollis* (AB032853), and *Rattus norvegicus* (DQ439844); arvicolinae rodents, including *Microtus arvalis* (EU439459), *Myodes glareolus* (DQ090761), and *Microtus pennsylvanicus* (AF119279); and a neotominae rodent, *Peromyscus maniculatus* (AF119261), as well as crocidurinae shrews, including *Suncus murinus* (DQ630386), *Crocidura lasiura* (AB077071), and *Crocidura dsinezumi* (AB076837); and soricinae shrews, including *Anourosorex squamipes* (AB175091), *Blarina brevicauda* (DQ630416), *Sorex cinereus* (EU088305), *Sorex monticolus* (AB100273), *Sorex araneus* (DQ417719), *Sorex caecutiens* (AB028563), *Sorex unguiculatus* (AB028525), and *Sorex gracillimus* (AB175131). The numbers at each node are posterior node probabilities based on 30,000 trees: two replicate MCMC runs consisting of six chains of 3 million generations each sampled every 1,000 generations with a burn-in of 7,500 (25%). The scale bar indicates nucleotide substitutions per site.

plausible that ongoing exchanges of hantaviruses continues to drive their evolution.

In this regard, several rodent species may occasionally serve as reservoir hosts for the same hantavirus. For example, Vladivostok virus (VLAV) may be found in its natural host, the reed vole (*Microtus fortis*) (37–39), as well as an ancillary host, the tundra or root vole (*Microtus oeconomus*) (40). Similarly, the Maximowiczi vole (*Microtus maximowiczii*) is the natural reservoir of Khabarovsk virus (KHAV), which may also be harbored by *Microtus fortis* (10, 39, 40). Moreover, a KHAV-related hantavirus, named Topografov virus (TOPV), has also been found in the Siberian lemming (*Lemmus sibiricus*) (41). This is a far more extreme situation in which a hantavirus has switched from its natural rodent reservoir host and become well established in a rodent host of a different genus. Such host-switching or species-jumping events may account for the extraordinarily close phylogenetic relationship between TOPV and KHAV (41). That is, whereas *Lemmus* and *Microtus* are very distantly related, TOPV and KBRV are monophyletic.

In much the same way, as evidenced by the polyphylogenetic relationship between ASAV and other soricid-associated hantaviruses, the progenitor of ASAV may have 'jumped' from its natural soricine shrew host to establish itself in the Japanese shrew mole, or vice versa. That is, burrows and shallow tunnel systems excavated by Japanese shrew moles may be occasionally shared with sympatric species, including shrews, allowing opportunities for virus transmission through interspecies wounding or contaminated nesting materials. Such a host-switching event may have occurred in the distant past, possibly before the present-day Japanese shrew mole became endemic in Japan. Accordingly, intensive investigations of shrews in Japan and elsewhere in Far East Asia may provide further insights into the evolutionary origins of hantaviruses.

Materials and Methods

Trapping. Sherman traps (H.B. Sherman) and pit-hole traps were used to capture shrews and shrew moles in Japan between October 2006 and April 2008. Traps were set at intervals of 4 to 5 m during the evening hours of each day, over a four-day period, at sites in Hokkaido (Hamatonbetsu, Saruhutsu, and Nopporo) and Honshu (Nara and Mie), where soricomorphs had been captured. Species, gender, weight, reproductive maturity, and global positioning system (GPS) coordinates of each captured animal were recorded.

Specimen Processing. Lung tissues, dissected using separate instruments, were frozen on dry ice, and then stored at −80°C until used for testing. In some instances, portions of tissues were also placed in RNAlater RNA Stabilization Reagent (QIAGEN, Inc.) and processed for RT-PCR within 4 weeks of tissue collection.

RNA Extraction and cDNA Synthesis. Total RNA was extracted from tissues, by using the PureLink Microto-Midi total RNA purification kit (Invitrogen), in a laboratory in which hantaviruses had never been handled. cDNA was then prepared by using the SuperScript™ III RNase H- reverse transcriptase kit (Invitrogen) with a primer based on the conserved 5′-terminus of the S, M and L segments of hantaviruses (5′-TAGTAGTAGACTCC-3′).

RT-PCR. Touchdown-PCR was performed by using oligonucleotide primers designed from TPMV and other hantaviruses: S (outer: 5′-TAGTAGTAGACTCCT-TRAARAGC-3′ and 5′-AGCTCIGGATCCATITCATC-3′; inner: 5′-AGYCCIGTIATGRG-WGTIRTYGG-3′ and 5′-AIGAYTGRTARAAIGAIGAYTTYT T-3′); M (outer: 5′-GGACCAGGTGCADCTTGTGAAGC-3′ and 5′-GAACCCCADGCCCCITCYAT-3′; inner: 5′-TGTGTICCWGGITTYCATGGIT-3′ and 5′-CATGAYATCTCCAGGGTCHCC-3′); and L (outer: 5′-ATGTAYGTBAGTGCWGATGC-3′ and 5′-AACCADTCWGTYC-CRTCATC-3′; inner: 5′-TGCWGATGCHACIAARTGGTC-3′ and 5′-GCRTCRTCW-GARTGRTGDGCAA-3′).

First- and second-round PCR were performed in 20-μL reaction mixtures, containing 250 μM dNTP, 2.5 mM $MgCl_2$, 1 U of LA Taq polymerase (Takara) and 0.25 μM of each primer (24). Initial denaturation at 94°C for 2 min was followed by two cycles each of denaturation at 94°C for 30 sec, two-degree step-down annealing from 46°C to 38°C for 40 sec, and elongation at 72°C for 1 min, then 30 cycles of denaturation at 94°C for 30 sec, annealing at 42°C for 40 sec, and elongation at 72°C for 1 min, in a GeneAmp PCR 9700 thermal cycler (Perkin–Elmer). PCR products were separated by agarose gel electrophoresis and purified by using the Qiaex Gel Extraction Kit (Qiagen). Amplified DNA was sequenced directly by using an ABI Prism 3130 Avant Genetic Analyzer (Applied Biosystems).

Genetic and Phylogenetic Analyses. Sequences were processed by using the Genetyx version 9 software (Genetyx Corporation) and aligned using Clustal W and W2 (42). For phylogenetic analysis, ML consensus trees were generated by the Bayesian Metropolis–Hastings Markov Chain Monte Carlo (MCMC) tree-sampling methods as implemented by Mr. Bayes (43) using a GTR + I + G model of evolution, as selected by hierarchical likelihood-ratio test (hLRT) in MrModeltest2.3 (http://www.abc.se/~nylander/mrmodeltest2/mrmodeltest2.html) (44), partitioned by codon position.

An initial ML estimate of the model of evolutionary change among aligned viruses was generated by MrModeltest2.3. ML tree estimation in PAUP (45) was conducted starting with a neighbor-joining (NJ) tree based on this initial ML model of evolution, and proceeding with successive rounds of heuristic tree-searches to select the single most likely ML tree. Support for topologies was generated by bootstrapping for 1,000 NJ replicates (under the ML model of evolution, implemented in

PAUP) and for 100 ML replicates (data not shown). Phylogenetic relationships were further confirmed using amino acid sequences analyzed by Bayesian tree sampling, using the WAG model (46) implemented by Bayes (43).

Secondary Structure Prediction. Secondary structure prediction of the N protein was performed using the NPS@ structure server (47). To achieve 70–80% accuracy and to validate the prediction, five different methods were used jointly: DSC (48), HNN (49), PHD (50), PREDATOR (51), and MLRC (49), which in turn were based on GOR4 (52), SIMPA96 (53), and SOPMA (54). The minimum number of conformational states was set to four (helix, sheet, turn, and coil) for each analysis, and the results were combined into a consensus structure where the most prevalent predicted conformational state was reported for each residue. For convenience in visualization of the predicted structures, the NPS@ server also provided graphic outputs for the individual sequences which were subsequently combined into a multipart joint image.

PCR Amplification of Shrew Mole mtDNA. Total DNA, extracted from liver tissues using the QIAamp Tissue Kit (QIAGEN), was used to verify the identity of the hantavirus-infected shrew moles. The 1,140-nucleotide mtDNA cytochrome *b* gene was amplified by PCR, using described universal primers (5′- CGAAGCTT-GATATGAAAAACCATCGTTG-3′; 5′- AACTGCAGTCATCTCCGGTTTACAAGAC-3′) (55). PCR was performed in 50-μl reaction mixtures, containing 200 μM dNTP and 1.25 U of rTaq polymerase (Takara). Cycling conditions consisted of an initial denaturation at 95°C for 4 min followed by 40 cycles with denaturation at 94°C for 1 min, annealing at 57°C for 1 min, and elongation at 72°C for 1 min in a GeneAmp PCR9700 thermal cycler.

ACKNOWLEDGMENTS. We thank Dr. Akio Shinohara (Frontier Science Research Center, University of Miyazaki) for kindly providing the photo of the Japanese shrew mole (Fig. 1). This work was supported by a Grant-in-Aid for Scientific Research (B) from the Ministry of Education, Science, and Culture of Japan (18300136), Gakujyutsu-Frontier Cooperative Research at Rakuno Gakuen University, and National Institute of Allergy and Infectious Diseases Grant R01AI075057, Centers of Biomedical Research Excellence Grant P20RR018727, and Research Centers in Minority Institutions Grant G12RR003061 from the National Center for Research Resources, National Institutes of Health.

1. Yanagihara R (1990) Hantavirus infection in the United States: Epizootiology and epidemiology. *Rev Infect Dis* 12:449–457.
2. Yanagihara R, Gajdusek DC (1988) in *CRC Handbook of Viral and Rickettsial Hemorrhagic Fevers*, ed Gear JHS (CRC Press, Boca Raton), pp 151–188.
3. Lee HW, Lee P-W, Johnson KM (1978) Isolation of the etiologic agent of Korean hemorrhagic fever. *J Infect Dis* 137:298–308.
4. Schmaljohn CS, Hasty SE, Harrison SA, Dalrymple JM (1983) Characterization of Hantaan virions, the prototype virus of hemorrhagic fever with renal syndrome. *J Infect Dis* 148:1005–1012.
5. Brummer-Korvenkontio M, *et al.* (1980) Nephropathia epidemica: Detection of antigen in bank voles and serologic diagnosis of human infection. *J Infect Dis* 141:131–134.
6. Lee HW, Baek LJ, Johnson KM (1982) Isolation of Hantaan virus, the etiologic agent of Korean hemorrhagic fever from wild urban rats. *J Infect Dis* 146:638–644.
7. Lee P-W, *et al.* (1985) Partial characterization of Prospect Hill virus isolated from meadow voles in the United States. *J Infect Dis* 152:826–829.
8. Avsic-Zupanc T, *et al.* (1992) Characterization of Dobrava virus: A hantavirus from Slovenia, Yugoslavia. *J Med Virol* 38:132–137.
9. Plyusnin A, *et al.* (1994) Tula virus: A newly detected hantavirus carried by European common voles. *J Virol* 68:7833–7839.
10. Hörling J, *et al.* (1996) Khabarovsk virus: A phylogenetically and serologically distinct hantavirus isolated from *Microtus fortis* trapped in far-east Russia. *J Gen Virol* 77:687–694.
11. Nemirov K, *et al.* (1999) Isolation and characterization of Dobrava hantavirus carried by the striped field mouse (*Apodemus agrarius*) in Estonia. *J Gen Virol* 80:371–379.
12. Baek LJ, *et al.* (2006) Soochong virus: A genetically distinct hantavirus isolated from *Apodemus peninsulae* in Korea. *J Med Virol* 78:290–297.
13. Duchin JS, *et al.* (1994) Hantavirus pulmonary syndrome: A clinical description of 17 patients with a newly recognized disease. *N Engl J Med* 330:949–955.
14. Nichol ST, *et al.* (1993) Genetic identification of a hantavirus associated with an outbreak of acute respiratory illness. *Science* 262:914–917.
15. Plyusnin A, Vapalahti O, Vaheri A (1996) Hantaviruses: Genome structure, expression and evolution. *J Gen Virol* 77:2677–2687.
16. Hughes AL, Friedman R (2000) Evolutionary diversification of protein-coding genes of hantaviruses. *Mol Biol Evol* 17:1558–1568.
17. Carey DE, Reuben R, Panicker KN, Shope RE, Myers RM (1971) Thottapalayam virus: A presumptive arbovirus isolated from a shrew in India. *Indian J Med Res* 59:1758–1760.
18. Zeller HG, *et al.* (1989) Electron microscopic and antigenic studies of uncharacterized viruses. II. Evidence suggesting the placement of viruses in the family *Bunyaviridae*. *Arch Virol* 108:211–227.
19. Song J-W, Baek LJ, Schmaljohn CS, Yanagihara R (2007) Thottapalayam virus: A prototype shrewborne hantavirus. *Emerg Infect Dis* 13:980–985.
20. Yadav PD, Vincent MJ, Nichol ST (2007) Thottapalayam virus is genetically distant to the rodent-borne hantaviruses, consistent with its isolation from the Asian house shrew (*Suncus murinus*). *Virol J* 4:80.
21. Song J-W, *et al.* (2007) Newfound hantavirus in Chinese mole shrew, Vietnam. *Emerg Infect Dis* 13:1784–1787.
22. Song J-W, *et al.* (2007) Seewis virus, a genetically distinct hantavirus in the Eurasian common shrew (*Sorex araneus*). *Virol J* 4:114.
23. Arai S, *et al.* (2007) Hantavirus in northern short-tailed shrew, United States. *Emerg Infect Dis* 13:1420–1423.
24. Arai S, *et al.* (2008) Phylogenetically distinct hantaviruses in the masked shrew (*Sorex cinereus*) and dusky shrew (*Sorex monticolus*) in the United States. *Am J Trop Med Hyg* 78:348–351.
25. Tkachenko EA, *et al.* (1983) Potential reservoir and vectors of haemorrhagic fever with renal syndrome (HFRS) in the U.S.S.R. *Ann Soc Belg Med Trop* 63:267–269.
26. Clement J, *et al.* (1994) in *Virus Infections of Rodents and Lagomorphs*, ed Horzinek MC (Elsevier Science BV, Amsterdam), pp 295–316.
27. Gavrilovskaya IN, *et al.* (1983) Features of circulation of hemorrhagic fever with renal syndrome (HFRS) virus among small mammals in the European U.S.S.R. *Arch Virol* 75:313–316.
28. Gligic A, *et al.* (1992) Hemorrhagic fever with renal syndrome in Yugoslavia: Epidemiologic and epizootiologic features of a nationwide outbreak in 1989. *Eur J Epidemiol* 8:816–825.
29. Ishii N (1993) Size and distribution of home ranges of the Japanese shrew-mole *Urotrichus talpoides*. *J Mamm Soc Jpn* 18:87–98.
30. Yokohata Y (2005) A brief review of the biology on moles in Japan. *Mammal Study* 30:S25–S30.
31. Shinohara A, Campbell KL, Suzuki H (2003) Molecular phylogenetic relationships of moles, shrew moles, and desmans from the new and old worlds. *Mol Phylogenet Evol* 27:247–258.
32. Shinohara A, Campbell KL, Suzuki H (2005) An evolutionary view on the Japanese talpids based on nucleotide sequences. *Mammal Study* 30:S19–S24.
33. Kawada S, Obara Y (1999) Reconsideration of the karyological relationship between two Japanese species of shrew-moles, *Dymecodon pilirostris* and *Urotrichus talpoides*. *Zoolog Sci* 16:167–174.
34. Harada M, Ando A, Tsuchiya K, Koyasu K (2001) Geographic variation in chromosomes of the greater Japanese shrew-mole, *Urotrichus talpoides* (Mammalia: Insectivora) *Zoolog Sci* 18:433–442.
35. Okumura M, *et al.* (2007) Development of serological assays for Thottapalayam virus, an insectivore-borne hantavirus. *Clin Vaccine Immunol* 14:173–181.
36. Klempa B, *et al.* (2007) Novel hantavirus sequences in shrew, Guinea. *Emerg Infect Dis* 13:520–552.
37. Kariwa H, *et al.* (1999) Genetic diversities of hantaviruses among rodents in Hokkaido, Japan and Far East Russia. *Virus Res* 59:219–228.
38. Zou Y, *et al.* (2008) Isolation and genetic characterization of hantaviruses carried by Microtus voles in China. *J Med Virol* 80:680–688.
39. Zou Y, *et al.* (2008) Genetic analysis of hantaviruses carried by reed voles Microtus fortis in China. *Virus Res* 137:122–128.
40. Plyusnina A, *et al.* (2008) Genetic analysis of hantaviruses carried by *Myodes* and *Microtus* rodents in Buryatia. *Virol J* 5:4
41. Vapalahti O, *et al.* (1999) Isolation and characterization of a hantavirus from *Lemmus sibiricus*: Evidence for host switch during hantavirus evolution. *J Virol* 73:5586–5592.
42. Thompson JD, Higgins DG, Gibson TJ (1994) CLUSTAL W: Improving the sensitivity of progressive multiple sequence alignment through sequence weighting, position-specific gap penalties and weight matrix choice. *Nucl Acids Res* 22:4673–4680.
43. Ronquist F, Huelsenbeck JP (2003) MrBayes 3: Bayesian phylogenetic inference under mixed models. *Bioinformatics* 19:1572–1574.
44. Posada D, Crandall KA (1998) MODELTEST: Testing the model of DNA substitution. *Bioinformatics* 14:817–818.
45. Swofford DL (2003) PAUP*. Phylogenetic analysis using parsimony (*and other methods). Version 4 (Sinauer Associates, Sunderland, Massachusetts).
46. Whelan S, Goldman N (2001) A general empirical model of protein evolution derived from multiple protein families using a maximum-likelihood approach. *Mol Biol Evol* 18:691–699.
47. Combet C, Blanchet C, Geourjon C, Deléage G (2000) NPS@: Network Protein Sequence Analysis. *Trends Biochem Sci* 25:147–150.
48. King RD, Sternberg MJ (1996) Identification and application of the concepts important for accurate and reliable protein secondary structure prediction. *Protein Sci* 5:2298–2310.
49. Guermeur Y, Geourjon C, Gallinari P, Deléage G (1999) Improved performance in protein secondary structure prediction by inhomogeneous score combination. *Bioinformatics* 15:413–421.
50. Rost B, Sander C (1993) Prediction of protein secondary structure at better than 70% accuracy. *J Mol Biol* 232:584–599.
51. Frishman D, Argos P (1996) Incorporation of non-local interactions in protein secondary structure prediction from the amino acid sequence. *Protein Eng* 9:133–142.
52. Garnier J, Gibrat J-F, Robson B (1996) GOR method for predicting protein secondary structure from amino acid sequence. *Methods Enzymol* 266:540–553.
53. Levin JM, B. Robson B, Garnier J (1986) SIMPA96: An algorithm for secondary structure determination in proteins based on sequence similarity. *FEBS Lett* 205:303–308.
54. Geourjon C, Deléage G (1995) SOPMA: Significant improvements in protein secondary structure prediction by consensus prediction from multiple alignments. *Comput Appl Biosci* 11:681–684.
55. Irwin DM, Kocher TD, Wilson AC (1991) Evolution of the cytochrome b gene of mammals. *J Mol Evol* 32:128–144.

Japanese Journal of Veterinary Research 55(4): 115-127, 2008

FULL PAPER

Characterization and epitope mapping of monoclonal antibodies to the nucleocapsid protein of severe acute respiratory syndrome coronavirus

Hiroaki Kariwa[1,*], Hiroshi Noda[1], Mina Nakauchi[1], Mariko Ishizuka[1], Kazuaki Hashiguchi[1], Shingo Hashimoto[1], Kentaro Yoshii[1], Atsushi Asano[2], Takashi Agui[2], Hiroyuki Kogaki[3], Yoshihiro Kurano[3], Yoshiaki Uchida[3], Nobuyuki Fujii[3], Masahisa Okada[3] and Ikuo Takashima[1]

[1]Laboratory of Public Health, Department of Environmental Veterinary Sciences, Graduate School of Veterinary Medicine, Hokkaido University, Sapporo 060-0818, Japan

[2]Laboratory of Experimental Animal Science, Department of Disease Control, Graduate School of Veterinary Medicine, Hokkaido University, Sapporo 060-0818, Japan

[3]Research and Development Division, Fujirebio Inc., Hachioji 192-0031, Japan

Received for publication, December 10, 2007; accepted, February 6, 2008

Abstract

The sudden emergence of severe acute respiratory syndrome (SARS) at the end of 2002 resulted in 774 reported deaths from more than 8000 cases worldwide. As no effective vaccines or antiviral agents are available, the most effective measure to prevent the expansion of a SARS epidemic is the rapid diagnosis and isolation of SARS patients. To establish specific diagnostic methods, we generated nine clones of monoclonal antibodies to nucleocapsid protein (NP) of SARS-coronavirus (SARS-CoV). On immunofluorescent antibody assay and Western blotting analysis, none of the monoclonal antibodies showed cross-reactivity to authentic and recombinant NPs of human coronavirus (HCoV) 229E strain. To determine the region on the NP molecule where the monoclonal antibodies bind, we generated four truncated recombinant NPs and analyzed the reactivity between monoclonal antibodies and truncated NPs. Two monoclonal antibodies reacted with a truncated NP covering from amino acid residues 111 to 230, and seven reacted with another truncated NP covering from amino acid residues 221 to 340. Epitope mapping analysis indicated that monoclonal antibody SN5-25 recognized the amino acid sequence Q^{245}TVTKK^{250} on SARS-NP. Within the epitope, Q245, T246, V247, K249, and K250 appeared to form an essential motif for monoclonal antibody SN5-25 to bind. The information about binding sites and epitopes of monoclonal antibodies may be useful for the development of new diagnostic methods for SARS and for analyzing the function of N protein of SARS-CoV.

Key Words: severe acute respiratory syndrome (SARS), coronavirus, nucleocapsid, epitope, monoclonal antibody

*Corresponding author: Hiroaki Kariwa, D.V.M., Ph.D., Laboratory of Public Health, Department of Environmental Veterinary Sciences, Graduate School of Veterinary Medicine, Hokkaido University, Sapporo 060-0818, Japan

Phone: +81-11-706-5212. Fax: +81-11-706-5213. E-mail: kariwa@vetemed.hokudai.ac.jp

Introduction

In late 2002, a severe respiratory illness of unknown etiology emerged in Guangdong Province, China, and spread to many parts of the world[18,20,28,29]. In March 2003, the World Health Organization (WHO) issued global alerts and designated the disease severe acute respiratory syndrome (SARS). A global research network funneled information to WHO. In April 2003, a novel coronavirus, designated SARS-coronavirus (SARS-CoV), was isolated as the causative agent[1,10,19]. By the time the epidemic was confined in July 2003, the number of probable cases had mounted to more than 8000, with 773 deaths in 32 countries or regions[26]. Several additional cases in Guangdong were later reported, as were laboratory-acquired infections in Singapore, Taipei, and Beijing.

Coronaviruses (*genus Coronavirus*, family *Coronaviridae*) generally target respiratory and intestinal tract organs. Although coronaviruses have traditionally been classified into three groups, based on their antigenic characterization, SARS-CoV appears to be distant from these groups, and was classified into a novel coronavirus group[16,21]. Coronaviruses were thought to be species-specific, but SARS-CoV infected monkeys, cats, ferrets, mice, and rats, as well as humans. The virus was identified in masked palm civets and raccoon dogs in a Guangdong animal market[4], as well as dogs and cats during the 2003 Amoy Gardens epidemic in Hong Kong[17]. Recent studies suggested that horseshoe bats may carry SARS-CoV-related viruses[11,13].

With a spherical virion 100-200 nm in diameter, a coronavirus has a positive sense, single-stranded genomic RNA, wrapped in an envelope. The three envelope proteins are spike (S) protein, responsible for large projections from the envelope; membrane (M) protein; and envelope (E) protein. S protein binds the virion to cells and is the target of neutralizing antibodies. Inside the virion, the viral genome is associated with nucleocapsid protein (NP). The functions of NP may be related to viral RNA replication, transcription, and RNA packaging[6,7,14,23,27]. As large amounts of NP are produced in infected cells[9,21], and anti-NP antibodies have been detected in more than 90% of patients[5,12,22,24,25], NP may be an appropriate immune response target.

Kogaki *et al.*[8] expressed NP in *E. coli* and produced monoclonal antibodies to NP to establish a diagnostic method for SARS. Their findings suggested that monoclonal antibodies can detect SARS-CoV NP with high sensitivity. Here we characterized these monoclonal antibodies by analyzing the binding sites and epitopes of the monoclonal antibodies to SARS-CoV NP. This analysis may clarify the significance of the monoclonal antibodies as SARS-CoV-specific diagnostic reagents and tools for analyzing the function of SARS-CoV NP.

Materials and methods

Cells and viruses

Vero E6 cells were cultured in Eagle's minimum essential medium (MEM) supplemented with 0.292 g/l L-glutamine and 5% heat-immobilized fetal bovine serum (FBS). The Hanoi strain of SARS-CoV was kindly provided by Dr. Koichi Morita, Nagasaki University, Japan, and propagated in Vero E6 cells. A monolayer of Vero E6 cells was infected with SARS-CoV and cultured for 2 days at 37℃ in a CO_2 incubator. The culture fluid of the infected cells was collected and centrifuged at 700×g for 5 min. The supernatant was stored at −80℃ as stock virus. The SARS-CoV-infected cells were transferred to sample tubes with a cell scraper. The cells were washed with phosphate-buffered saline (PBS), and the pellets were stored at −80℃ until use. L132 cells and the human coronavirus (HCoV) 229E strain were kindly provided by Dr. Shigeru Morikawa, National Institute of Infectious Diseases, Japan. The L132 cells were cultured in Dulbecco's modified Eagle's medium (DMEM) with 0.292 g/l L-glutamine and 5% FBS. They were then infected with HCoV 229E and cultured for 3 days at 37℃ in

a CO_2 incubator. The culture fluid and HCoV 229E -infected cells were collected as described above.

Establishment of monoclonal antibodies to SARS-CoV NP

The cDNA of SARS-CoV Urbani strain NP was prepared from synthetic oligonucleotides and polymerase chain reaction (PCR), using Pfu Taq DNA polymerase[2]. The cDNA was cloned into the pW6A vector, and the plasmid containing the SARS-CoV NP gene was designated pWSN. The recombinant SARS-CoV NP was expressed in *E. coli* BL 21 cells and purified by DEAE-Sepharose (Whatman DE52) ion exchange chromatography and Phenyl-Sepharose Fast Flow (Pharmacia) chromatography[3]. We prepared mouse monoclonal antibodies to both the purified NP and a synthetic peptide (GQTVTKKSAAEASKKPR) that was equivalent to the amino acid sequence (244-260 aa) of the Urbani strain NP[6], thus establishing monoclonal antibodies rSN16a, rSN17, rSN18, rSN21, rSN21-2, rSN113, and rSN150 against the purified recombinant NP and monoclonal antibody SN5-25 against the synthetic peptide. The monoclonal antibodies used in this study are listed in Table 1.

Preparation of rabbit immune serum

A Japanese white rabbit (Japan SLC Inc.) was immunized with recombinant NP six times at 2-week intervals. At the first immunization, recombinant NP mixed with complete Freund's adjuvant was injected into the animal. In the latter five immunizations, recombinant NP mixed with incomplete Freund's adjuvant was injected. The rabbit was sacrificed by cardiac puncture under anesthesia, and the collected rabbit serum was heat-inactivated at 56℃ for 30 min and stored at −40℃ until use. All animal experiments were performed according to the guidelines of the Graduate School of Veterinary Medicine, Hokkaido University, Japan.

Reverse transcriptase-polymerase chain reaction (RT-PCR)

Total RNA was isolated with Isogen (Nippon Gene), according to the manufacturer's protocol. The reverse transcription mixture was prepared in a tube by adding 4 μl of 5× first-strand buffer, 2 ml 0.1M dithiothreitol, 1μl 10 mM dNTP mixture, 1 μl of 50 μM oligo dT_{20} (Invitrogen), 1 μl of sample RNA solution containing 1 μg of total RNA, and diethylpyrocarbonate-treated water, for a final volume of 19 μl. The mixture was heated at 70℃ for 10 min and kept at 42℃ for 2 min, after which 1 μl (200 units) of Superscript II (Invitrogen) was added. The tube was maintained at 42℃ for 50 min, heated at 70℃ for 15 min, and then used as cDNA.

Table 1. Monoclonal antibodies used in this study

Name	Immunogen	Source
rSN16a	Recombinant SARS-CoV NP[a]	This report
rSN17	Recombinant SARS-CoV NP	This report
rSN18	Recombinant SARS-CoV NP	Kogaki et al[6]
rSN21	Recombinant SARS-CoV NP	This report
rSN21-2	Recombinant SARS-CoV NP	Kogaki et al[6]
rSN113	Recombinant SARS-CoV NP	This report
rSN122	Recombinant SARS-CoV NP	Kogaki et al[6]
rSN150	Recombinant SARS-CoV NP	Kogaki et al[6]
SN5-25	Synthetic peptide[b]	Kogaki et al[6]

[a] Full length SARS-CoV NP expressed in *E. coli*.

[b] Synthetic peptide (GQTVTKKSAAEASKKPR) equivalent to amino acid residues 244-260 of SARS-CoV Urbani strain NP.

Amplification of full-length and truncated SARS-CoV N protein genes

The PCR mixture was prepared in 0.2-ml tubes, with addition of 0.5 μl of 5 U/μl Platinum Taq polymerase HiFi (Invitrogen), 5 μl of 10× HIFI buffer, 1 μl of 10 mM dNTP, 2 μl of 50 mM $MgSO_4$, 37.5 μl of water, 1μl of 10 mM primers, and 2 μl of cDNA. PCR was performed at 94℃ for 2 min, followed by 35 thermal cycles of 94℃ for 2 min, 60℃ for 30 s, and 68℃ for 30 s. The regions of amplified NP genes were nucleotide residues 1-1269 (NP Full), 1-360 (trNP1), 331-690 (trNP2), 661-1020 (trNP3), and 991-1269 (trNP4; Fig. 1).

Cloning of SARS-CoV NP genes

To add the one adenine base overhang at the 3' end of the amplified DNA fragments, 0.25 μl of Ampli Taq (Applied Biosystems) was added to the PCR mixture and kept at 70℃ for 10 min. The amplified DNA fragments were electrophoresed in SeaKem GTG agarose gels (Cambrex). DNA fragments of the correct molecular size were cut from the gel and purified using a QIAquick Gel Extraction Kit (Qiagen), according to the manufacturer's instructions. The purified DNA fragments were ligated with the pCR2.1 vector using a TA Cloning Kit (Invitrogen). Plasmids containing the NP gene were obtained from the cultures of transformed TOP10F' (Invitrogen) *E. coli* cells, and the NP gene inserts in the plasmids were sequenced. The nucleotide sequence of the Hanoi strain N gene perfectly matched that of the SARS-CoV Urbani strain [AY278741]. The plasmids with the NP genes and pET43.1a (Novagen) were digested with *Pst*I and *Eco*RI. The NP gene and pET43.1a were then ligated using a DNA Ligation Kit (Takara Bio Inc.).

Expression of recombinant NP

The pET43.1a plasmids containing NP genes were selected, multiplied, and purified as described above. *Escherichia coli* AD494pLys cells were transformed with the plasmids and cultured at 37℃ overnight in 2 ml of Luria-Bertani (LB) medium with 50 μg of ampicillin. The bacterial cultures (40 μl) were inoculated into 4 ml of fresh LB medium and cultured at 37℃ for 3 h. IPTG was added to the cultures, and the bacteria were

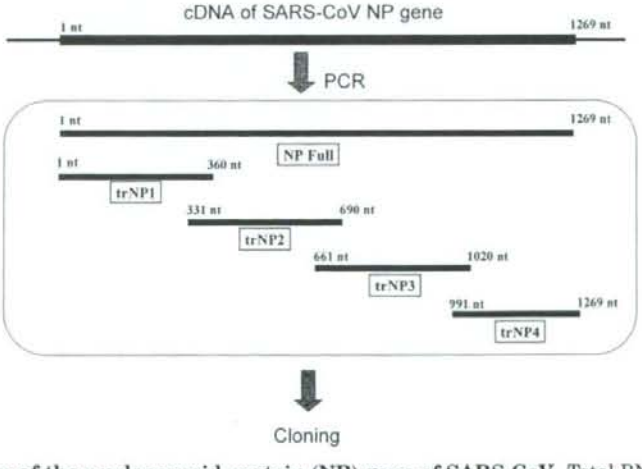

Fig. 1. Amplification of the nucleocapsid protein (NP) gene of SARS-CoV. Total RNA from infected Vero E6 cells was subjected to reverse transcription. The regions of NP genes amplified by PCR were nucleotide residues 1-1269 (NP Full), 1-360 (trNP1), 331-690 (trNP2), 661-1020 (trNP3), and 991-1269 (trNP4). The amplified DNA fragments were ligated into the pCR2.1 vector using a TA Cloning Kit (Invitrogen), and sequenced. The plasmids with the NP genes and pET43.1a (Novagen) were digested with *Pst*I and *Eco*RI. The digested NP genes were cloned into pET43.1a.

further cultured for 3 h. After culturing, the bacteria were collected by centrifugation at 5000 × g for 5 min and washed with 1 ml of 20 mM Tris-HCl (pH 8.0). The bacterial pellets were lysed with 400 µl of BugBuster reagent (Novagen) and 4 µl of Benzonuclease (Invitrogen) at room temperature for 20 min. After centrifugation at 16000 × g at 4℃ for 20 min, the supernatant was filtered through a 0.45-µm pore size membrane filter (Millipore), and used as the crude protein fraction. The recombinant NP was purified using ProBond resin (Invitrogen), according to the manufacturer's instructions. Briefly, aliquots of 300 µl of the resin were washed once in 2.0-ml tubes with 600 µl of water and equilibrated three times with 20 mM imidazole binding buffer. The soluble proteins were added to the resin and kept at 4℃ for 1 h. After centrifugation at 4℃ for 1 min, the resin was washed four times with 600 µl of 60 mM imidazole binding buffer. Finally, 1 ml of 300 mM imidazole binding buffer was added to the resin, mixed at 4℃ for 10 min, and the supernatant was collected as recombinant NP solution. The SARS-CoV NPs NP Full, trNP1, trNP2, trNP3, and trNP4 were expressed as fusion proteins with an NusA tag.

Western blotting analysis

Recombinant NPs were subjected to SDS-polyacrylamide gel electrophoresis (SDS-PAGE) and blotted onto polyvinylidene difluoride (PVDF) membranes (Immunobilon PVDF, Millipore). The membranes were blocked with BlockAce (Dainippon Pharmaceutical Co. Ltd.) at 4℃ overnight and washed with Tris-buffered saline (TBS: 25 mM Tris-HCl, pH7.4, and 150 mM NaCl). After washing three times with a mixture of TBS and 0.05% Tween 20 mixture (TBST), the membranes were immersed in 1:500-diluted mouse monoclonal antibody to SARS-CoV NP at 37℃ for 1 h. After washing with TBST, the membranes were immersed in 1:2000-diluted alkaline phosphatase-conjugated anti-mouse IgG (Jackson ImmunoResearch Laboratory Inc.) at 37℃ for 1 h. The membranes were washed five times, and the bands were visualized using an AP Detection Reagent Kit (Novagen).

Enzyme-linked immunosorbent assay (ELISA)

Recombinant NP-NusA and NusA proteins were diluted with carbonate buffer (Sigma-Aldrich), and 50-µl aliquots of these solutions were added to 96-well assay plates at 4℃ overnight. The plates were washed five times with PBS containing 0.05% Tween 20 (PBST) and blocked with 200 µl of 1:4-diluted BlockAce (Dainippon Pharmaceutical Co. Ltd.) at 37℃ for 1 h. The plates were washed five times and reacted with 50 µl/well of monoclonal antibodies diluted 1:1000 with 0.5% bovine serum albumin (BSA) in PBST (BSA-PBST) at 37℃ for 1 h. After washing, 50 µl/well of peroxidase-conjugated anti-mouse IgG (Jackson ImmunoResearch Laboratory Inc.), diluted at 1:5000 with BSA-PBST, were applied to the plates, which were then incubated at 37℃ for 1 h. After washing, 100 µl o-phenylenediamine (Sigma-Aldrich) with H_2O_2 were added to the plates, which were then left at room temperature for 30 min. The optical densities at 450 nm (OD_{450}) and 620 nm (OD_{650}) were measured to calculate the ELISA value (OD_{450}-OD_{650}).

Indirect immunofluorescence assay (IFA)

Vero E6 cells grown on Lab-Tek eight-well chamber slides (Nalge Nunc) were infected with 3.52×10^4 tissue culture infective dose 50 ($TCID_{50}$) SARS-CoV at 37℃ for 1 h, after which 400 µl of minimal essential medium (MEM) were added to each well. The infected cells were cultured at 37℃ for 24 h in a CO_2 incubator, fixed with 800 µl of methanol per well, and irradiated with ultraviolet light for 30 min at room temperature. The fixed slides were stored at −40℃ until use. The monoclonal antibodies were serially diluted with PBS and applied to the slides (100 µl/well), which were then incubated at 37℃ for 1 h and washed three times with PBS. FITC-conjugated anti-mouse IgG antibody (MP Biomedicals) diluted with 1:400 PBS was added to the slides (100 µl/well). After washing, the slides were embedded with buffered glycerol (1 PBS:9 glycerol), covered with a cover glass, and observed with a confocal laser microscope.

Epitope mapping of monoclonal antibodies by the 9-fluorenylmethyloxycarbonyl (Fmoc) method

To determine the antibody epitopes on SARS-CoV NP, peptides consisting of ten NP amino acid residues were synthesized on membranes. All peptides were synthesized with an Autospot Peptide Synthesizer, ASP222 (AbiMED), using an Fmoc-protected system and Amino-Peg-membranes (INTAVIS Bioanalytical Instruments AG). The peptide-spotted membranes were rinsed once in methanol and twice in PBST. The membranes were blocked with BlockAce for 30 min at room temperature and washed three times with PBST. The membranes were soaked in 1:500-diluted monoclonal antibody, incubated at 37℃ for 60 min, and washed three times with PBST. The membranes were then soaked with 1:2000-diluted horseradish peroxidase-conjugated anti-mouse IgG (Jackson ImmunoResearch Laboratories), incubated at 37℃ for 60 min, and washed three times with PBST. To visualize peptide spots that reacted with the monoclonal antibodies, the membranes were stained with a 3-amino-9-ethylcarbazole (AEC) detection system (Sigma-Aldrich). After incubation with AEC reagent for a few minutes, the membranes were washed with distilled water and air-dried.

Results

Reactivity of monoclonal antibodies to authentic SARS-CoV and HCoV 229E NPs

To develop specific diagnostic methods for SARS, nine clones of mouse monoclonal antibodies to SARS-CoV NP were generated by immunizing a Japanese white rabbit with synthetic peptide or recombinant NP. To determine the reactivity of these monoclonal antibodies to authentic NP, Vero E6 cells infected with SARS-CoV were stained with monoclonal antibodies. Cells infected with SARS-CoV showed strong fluorescent signals with all of the antibodies, but neither cells infected with HCoV 229E strain nor normal cells showed a signal (Fig. 2). To determine the specificity of the antibodies in more detail, Western blotting analysis was performed. All antibodies showed a distinct signal at 46 KDa corresponding to NP in SARS-CoV-infected Vero E6 cells, but not in HcoV-229E-infected L132 cells or normal cells (Fig. 3). The NPs of SARS-CoV, HCoV 229E, and HCoV OC43 were expressed in bacterial cells, and the reactivities of these NPs to monoclonal antibodies were analyzed by Western blotting (Fig. 4). All nine monoclonal antibodies reacted only with SARS-CoV NP, and no cross-reactivity was observed with NPs of HCoV 229E or OC43 strains. In ELISA, all monoclonal antibodies reacted with full-length NP in a dose-dependent manner (Fig. 5).

Reactivity of monoclonal antibodies to truncated SARS-CoV NPs

To determine the binding regions of monoclonal antibodies on NP, four different truncated NPs (trNPs) were expressed as fusion proteins with an NusA tag in *E. coli*, and purified. On Western blots, two antibodies (rSN113 and rSN122) showed distinct signals with trNP2, covering NP amino acid residues 111-230 (Fig. 6). The remaining seven antibodies (SN5-25, rSN16a, rSN17, rSN18, rSN21, rSN21-2, and rSN150) showed a signal to trNP3 covering amino acid residues 221-340. In ELISA, rSN113 and rSN122 also showed signals to trNP2,and SN5-25 reacted with trNP3, but the remaining antibodies showed no reactivity to any of the trNPs (data not shown).

Epitope mapping by Fmoc solid-phase peptide synthesis

To determine the epitopes of the monoclonal antibodies, we performed epitope mapping using the Fmoc solid-phase peptide synthesis method. As SN5-25 was generated by immunization with the synthetic peptide GQTVTKKSAAEASKKPR, which was equivalent to amino acid residues 244-260 of NP, various ten-amino-acid peptides were synthesized from the 244-260 amino acid sequence of NP by spotting peptides of nine amino acids at various places on a membrane. Positive signals were observed at sites containing Q^{245}TVTKK^{250}

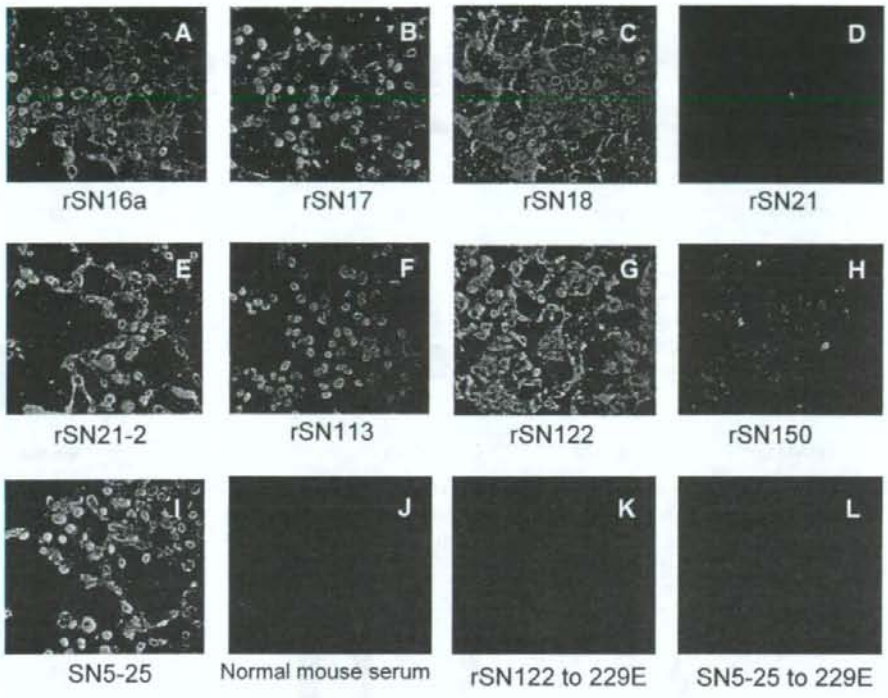

Fig. 2. Reactivity of monoclonal antibodies to SARS-CoV-infected Vero E6 cells. Vero E6 monolayers grown in an eight-chamber slide were infected with SARS-CoV Hanoi strain, and the cells were cultured at 37℃ for 1 day in a CO_2 incubator. The cells were fixed with methanol and reacted with the monoclonal antibodies. The reaction was visualized with FITC-conjugated anti-mouse IgG antibody and observed with a confocal laser microscope.

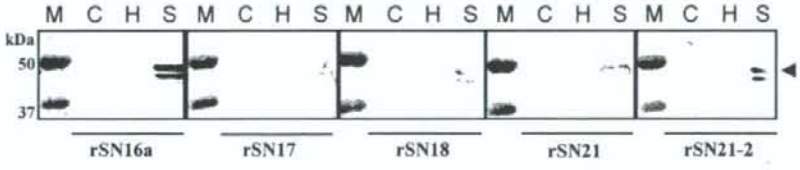

Fig. 3. Reactivity of monoclonal antibodies to authentic viral NPs on Western blotting analysis. Molecular marker (M), lysates of normal Vero E6 cells (C), human coronavirus 229E-infected L132 cells (H), and SARS-CoV-infected Vero E6 cells (S) were subjected to SDS-PAGE and transferred onto PVDF membranes. After reaction with the cell lysates, each monoclonal antibody was analyzed for binding specificity.

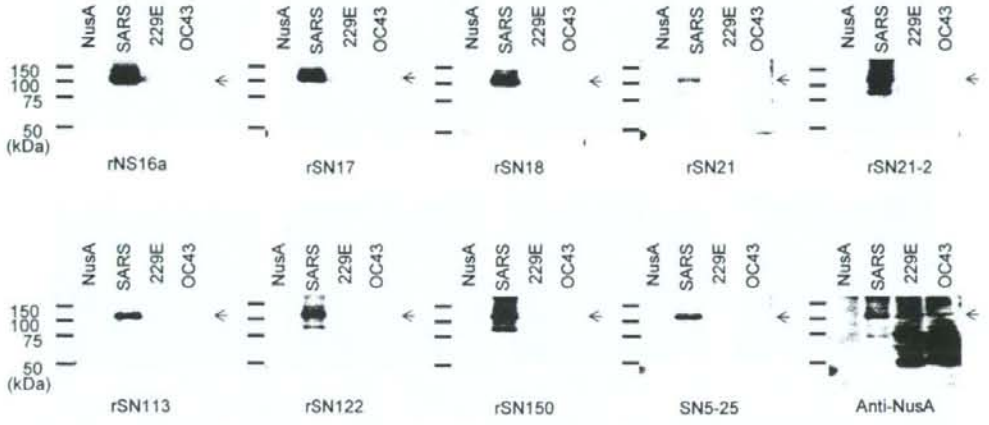

Fig. 4. Reactivity of monoclonal antibodies to recombinant NPs of SARS-CoV and human coronaviruses (HCoV). NPs of SARS-CoV, HCoV 229E, and HCoV OC43 were cloned into pET43.1a and expressed as fusion proteins with NusA protein in *E. coli*. The bacterial lysates were subjected to SDS-PAGE, transferred onto PVDF membranes, and analyzed by Western blotting.

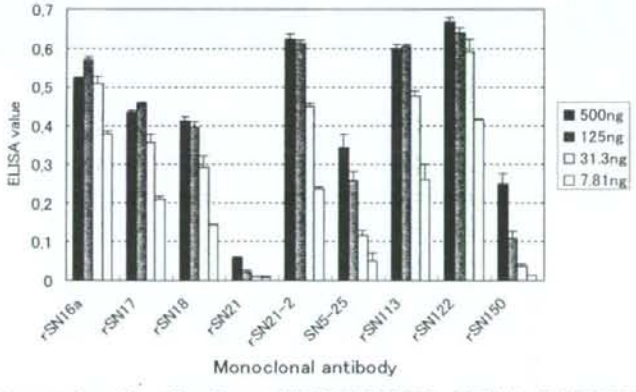

Fig. 5. Reactivity of monoclonal antibodies to SARS-CoV NP in ELISA. SARS-CoV NP was expressed as a fusion protein with NusA protein in *E. coli*. The bacterial lysate was purified and used as the antigen for ELISA. Full-length NP and NusA (2.5ng each) were used to coat plates and reacted with each monoclonal antibody in different amounts (7.82, 31.3, 125, and 500 ng/well). The ELISA values for each antibody were calculated as the differences in optical densities between wells with NP and NusA.

(Table 2), suggesting that this sequence is the epitope for monoclonal antibody SN5-25. To determine the essential amino acids in the epitope for monoclonal antibody SN5-25 binding, six amino acid peptides with substitutions of Alanine (A) were also analyzed for binding to SN5-25 (Table 3). Most of the substituted peptides lost reactivity, but QTVAKK reacted with SN5-25. Therefore, Q245, T246, V247, K249, and K250 appear to form an essential binding motif of SN5-25. We used the same strategy to search for the remaining eight monoclonal antibody epitopes, but found none. The NP gene amino acid sequence in the pET 43.1 vector was mutated by site-directed mutagenesis, yielding $A^{245}TVTKK^{250}$ and $Q^{245}TVTKA^{250}$, which lost reactivity in the Fmoc method. The lysates of the mutated plasmid-transformed *E. coli* did not react with SN5-25 on Western blotting analysis (data not shown).

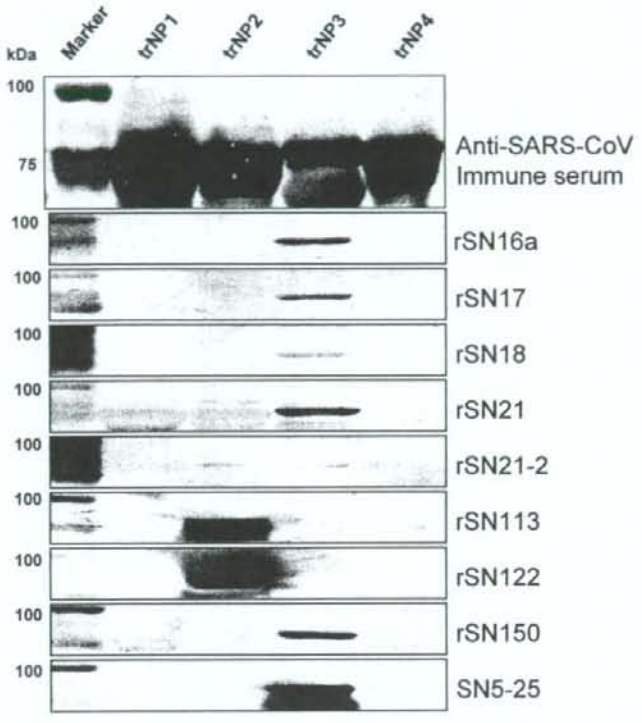

Fig. 6. Analysis of the regions on NP bound by the monoclonal antibodies. Four different truncated NPs were expressed as fusion proteins with NusA in *E. coli*, and the purified truncated NPs were subjected to SDS-PAGE. The truncated NPs were then transferred onto PVDF membranes, and the binding region of each monoclonal antibody was analyzed by Western blotting.

Table 2. Mapping of the epitope for SN5-25 monoclonal antibody on SARS-CoV NP[a]

Amino acid sequence on SARS-CoV NP	Position of amino acid residue	Reaction with SN5-25
QQQQGQTVTK	240-249	−
QQQGQTVTKK	241-250	+
QQGQTVTKKS	242-251	+
QGQTVTKKSA	243-252	+
GQTVTKKSAA	244-253	+
QTVTKKSAAE	245-254	+
TVTKKSAAEA	246-255	−
VTKKSAAEAS	247-256	−

[a] Peptides consisting of ten NP amino acid residues were synthesized on a membrane using an Fmoc-protected system. The peptide-spotted membrane was immunostained with an SN5-25, horseradish peroxidase-conjugated anti-mouse IgG, and 3-amino-9-ethylcarbazole detection system.